HHS Public Access
Author manuscript
Phytochemistry. Author manuscript; available in PMC 2020 March 01.

Published in final edited form as:
Phytochemistry. 2019 March ; 159: 75–89. doi:10.1016/j.phytochem.2018.12.007.

Temporal resistance of potato tubers: Antibacterial assays and metabolite profiling of wound-healing tissue extracts from contrasting cultivars

Keyvan Dastmalchi[^,†], **Mathiu Perez Rodriguez**[^,†], **Janni Lin**[†], **Barney Yoo**[£], and **Ruth E. Stark**[†,§,¶,*]

[†]Department of Chemistry and Biochemistry, The City College of New York, City University of New York and CUNY Institute for Macromolecular Assemblies, New York, NY 10031, USA

[£]Department of Chemistry, Hunter College of CUNY, New York, NY 10065, USA

[§]Ph.D. Program in Chemistry, CUNY Graduate Center, New York, NY 10016, USA

[¶]Ph.D. Program in Biochemistry, CUNY Graduate Center, New York, NY 10016, USA

Abstract

Solanum tuberosum, commonly known as the potato, is a worldwide food staple. During harvest, storage, and distribution the crop is at risk of mechanical damage. Wounding of the tuber skin can also become a point of entry for bacterial and fungal pathogens, resulting in substantial agricultural losses. Building on the proposal that potato tubers produce metabolites to defend against microbial infection during early stages of wound healing before protective suberized periderm tissues have developed, we assessed extracts of wound tissues from four potato cultivars with differing skin morphologies (Norkotah Russet, Atlantic, Chipeta, and Yukon Gold). These assays were conducted at 0, 1, 2, 3 and 7 days post wounding against the plant pathogen *Erwinia carotovora* and a non-pathogenic *Escherichia coli* strain that served as a control. For each of the potato cultivars, only polar wound tissue extracts demonstrated antibacterial activity. The polar extracts from earlier wound-healing time points (days 0, 1 and 2) displayed notably higher antibacterial activity against both strains than the later wound-healing stages (days 3 and 7). These results support a burst of antibacterial activity at early time points. Parallel metabolite profiling of the extracts revealed differences in chemical composition at different wound-healing time points and allowed for identification of potential marker compounds according to healing stage for each of the cultivars. It was possible to monitor the transformations in the metabolite profiles that could account for the phenomenon of temporal resistance by looking at the relative quantities of various metabolite classes as a function of time.

GRAPHICAL ABSTRACT

[*] rstark@ccny.cuny.edu, +1-212-650-8916.
[^]These two authors contributed equally to this work.

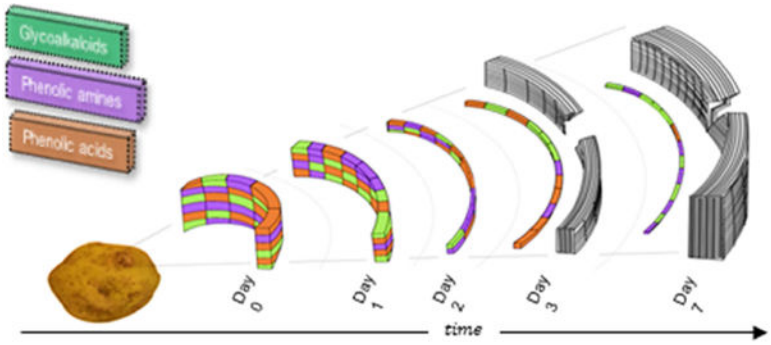

Keywords

Potato; *Solanum tuberosum*; wound periderm; temporal resistance; antibacterial; *Erwinia carotovora*; *Escherichia coli*; LC-MS, multivariate statistical analysis; biomarkers

1. Introduction

The potato *(Solanum tuberosum)* is an abundantly consumed food staple that nevertheless suffers from the loss of nearly half of harvested tubers on the way to market (Schieber & Saldana, 2008). Wounding of the skin surface represents a significant risk during cultivation, harvesting, and storage, given the susceptibility of this water-and starch-rich tissue to both desiccation and microbial invasion (Lulai, 2007). For instance, potatoes suffer from *Erwinia carotovora* and *Pectobacterium* bacterial infections in which pectin breakdown leads to soft rot or lenticel spot defects (van der Wolf & De Bore, 2007). The current lack of bactericides to treat these diseases represents a major agricultural concern but arguably also a phytochemical investigative opportunity, prompting us to seek a molecular-level definition of the natural defenses that can mitigate the impact of these problems.

Previously, we reported metabolic profiling of wound healing in potato tubers from four cultivars with contrasting skin characteristics (Dastmalchi, et al., 2014; Dastmalchi, et al., 2015). Periderm tissues at day 3 and day 7 post wound induction were investigated: the former time point is associated with the formation of a closing layer consisting of suberized phellem cells (‘primary suberization’) (Lulai, et al., 2016), whereas the latter time point is associated with the development of the wound periderm (‘secondary suberization’) (Lulai, 2007; Lulai & Corsini, 1998). Using bottom-up metabolomic analyses of polar and nonpolar wound tissue extracts, it was found that the profiles during closing layer formation at day 3 were quite distinct for four cultivars with skins that exhibited a gradient in russeting character. Upon initiation of wound periderm development at day 7, however, convergence rendered these compositional profiles less distinct (Dastmalchi, et al., 2014; Dastmalchi, et al., 2015). Completing this ‘holistic’ compositional analysis with solid-state ^{13}C NMR of the suberin-enriched cell-wall layer, significant differences were also observed among the four cultivars at both time points, with the most-and least-developed suberin biopolymers found in Yukon Gold and Atlantic cultivars, respectively (Dastmalchi, et al., 2015). During the course of these studies it became clear that the wound tissue at both healing time points produces a host of chemicals with established antioxidant, antimicrobial, and insecticidal

attributes (Dastmalchi, et al., 2014; Dastmalchi, et al., 2015). Some of the polar potato tissue extracts were found to have significant antioxidant properties, laying the groundwork for antioxidant fractionation studies of the most potent extracts (Dastmalchi, et al., 2016). Thus in addition to the suberin deposited within the phellem cells of the periderm (Lulai, 2007), plant protection could be conferred by the polar and nonpolar metabolites within the wound-healing tissues.

The hypothesis of early-onset defense by small molecules in potato tubers originated from a correlation, observed across a diverse series of potato genotypes, between robust temporal resistance directly after tuber wounding and the speed with which suberization is initiated (Lulai, 2007). This proposal was recently strengthened by measurements of increasing gene expression and associated production of particular polyamines during a 7-day time course after tissue wounding (Lulai, et al., 2015). To obtain a more complete picture of the chemical defenses and associated antimicrobial capabilities that protect the wounded tissues during a 2-day time course prior to closing layer formation, the current work applies the strategy demonstrated previously for tissue extracts from differently russeted cultivars (Dastmalchi, et al., 2014; Dastmalchi, et al., 2015; Huang, et al., 2017) and genetically modified potato varieties (Jin, et al., 2018) in conjunction with biological assays against Gram-negative bacteria.

First, we evaluated the ability of the wound tissue extracts to inhibit *Erwinia carotovora*, a major potato pathogen responsible for crop waste due to soft rot (des Essarts, et al., 2016; Toth, et al., 2003) and against which no effective controls are currently available (Czajkowski, et al., 2011). The antibacterial action against *E. carotovora* cultures was monitored during the logarithmic phase (log-phase) of growth for polar vs. nonpolar extracts. These assessments were compared at several post-injury time points leading up to the initiation of secondary suberization, and also as a function of cultivar in potato tubers with a gradient of russeting character. In parallel, comparative metabolite profiles were examined for periderm tissues at both early (days 0, 1 and 2) and late (days 3 and 7) wound-healing time points within each cultivar. In this way, it was possible to identify the principal chemical entities and transformations that control the phenomenon of temporal resistance upon wounding of potato tubers. These potential biomarker compounds can also be of significant importance in guiding the development of methods that expedite the process of wound healing in various potato cultivars (Dastmalchi, et al., 2015).

2. Results

2.1. Antibacterial Activity

The diminished absorbance readings at 600 nm for *E. coli* and *E. carotovora* bacterial strains incubated with day-0 polar extracts, with respect to methanol controls, are indicative of significant antibacterial activity of the Atlantic and Norkotah Russet cultivars, respectively (Fig. 1). These absorbance trends can be due either to lysis of the bacterial cells and/or inhibition of growth. Analogous behavior was observed for extracts obtained at days 1, 2, 3, and 7 after tuber tissue wounding (data not shown). The nonpolar extracts did not demonstrate antibacterial activity against either *E. coli* or *E. carotovora* (data not shown). To make a more quantitative assessment of these polar extract activities, percentage inhibition

values at the 6-hour exposure point, during the logarithmic phase of bacterial growth, were plotted for the *E. coli* (Figs. 1c, 2) and *E. carotovora* (Figs. 1d, 3) preparations.

For the *E. coli* standard Gram-negative bacteria the most potent wound tissue extracts belonged to the day-0 Norkotah Russet cultivar. Regardless of the specific inhibition values, however, a notable trend in growth inhibition was observed with increasing time after wounding: for each cultivar, a largely decreasing trend in extract activity was observed from the early (days 0–2) to late (days 3–7) wound-healing time points. Thus, the antibacterial capability of the polar wound tissue extracts against *E. coli* at the stage prior to closing layer formation generally exceeded the activity of the late wound-healing time points that are closer to the onset of secondary suberization.

On the other hand, *E. carotovora* showed a somewhat different pattern of results (Fig. 3). The most potent extract was derived from the day-0 Atlantic wound tissue. The time-dependent trend in antibacterial activity observed within each cultivar was more cleanly monotonic than that observed against *E. coli:* all cultivars displayed drop-offs at the later wound-healing stages. The decrease in activity was more pronounced for Atlantic and Yukon Gold cultivars.

It was also interesting to compare the cultivar-specific antibacterial activities at each wound-healing time point. Against *E. coli,* Norkotah Russet showed the highest antibacterial activity at day 0, whereas Chipeta was most active at days 1, 2 and 3, and Atlantic at day 7. Against *E. carotovora*, the most potent cultivar also varied according to wound-healing time point: highest for Atlantic and Yukon at day 0, highest for Norkotah Russet at day 1, all similar at day 2, most potent for Norkotah Russet at days 3 and 7. Taken together, these results demonstrate early and robust antibacterial defense capability prior to protection of the plant tissues via suberization.

2.2. Microscopic Imaging

Although changes in absorbance of a cell culture are commonly used to assess antibacterial activity, it was also useful to monitor the cell lysis that underlies this assay and to test for other possible morphological changes that could result from exposure to the potato wound periderm extracts. Figs. 4 and 5 illustrate light microscope images obtained from *E. coli* and *E. carotovora* cultures incubated with the most potent antibacterial wound extracts, day-0 Atlantic (Wd0A) and day-0 Norkotah Russet (Wd0R), respectively. Both cell lysis and morphological modifications were observed.

For instance, Fig. 4 shows striking bacterial cell elongation and increased cell thickness of Wd0R-exposed *E. coli* even at the low 8 μg/mL concentration. Fig. 5 reveals lysis of *E. carotovora* with both low and high Wd0A concentrations; at the higher concentration (Fig. 5b), it is also possible to discern abnormal morphological changes such as cell elongation and increased cell thickness. For both Wd0A activity against *E. carotovora* and Wd0R activity against *E. coli*, use of even higher extract concentrations increased the prevalence of cell lysis and changes in appearance among the bacterial cells (data not shown). The morphological changes, which can have disparate effects on the measured absorbance values, could result from changes in cell permeability and prevention of bacterial division.

2.3. LC-MS Metabolite Profiling: Temporal Variation of Potential Biomarker Compounds

To explore the molecular basis for the observed antibacterial trends, we undertook chemical characterization of the polar extract mixtures, using LC-MS and multivariate statistical analysis to focus on their distinguishing features as a function of cultivar or time point after wounding. The principal component analysis (PCA) plot presented in Fig. 6 illustrates how the metabolite profiles of the Atlantic cultivar converge (or diverge) during the wound-healing time course. At earlier wound-healing time points (days 0 and 1), the profiles of the wound tissue extracts were clearly distinct. However as the wound healing progressed the metabolite profiles became more similar, though they remained distinct. This result, which differs from the complete day-7 convergence observed previously under somewhat different growth, environmental, and analysis conditions (Dastmalchi, et al., 2014). The variables PC1 and PC2 accounted for more than 62% cumulative variation among the samples. The orthogonal partial least squares discriminate analysis (OPLS-DA) plot of Fig. 6 shows the clear separation of day 0 from the remaining wound-healing time points, confirmed by R^2X and R^2Y values of 0.82 and 0.99, respectively

The potential marker compounds contributing to the compositional differences among the polar cultivar extracts were derived from OPLS-DA analysis and the associated scatter plots (S-plots) as described previously (Dastmalchi, et al., 2014; Dastmalchi, et al., 2015). Finally, a variable line plot was used to verify the specificity of each potential biomarker to the cultivar type. Fig. 7 and Table 1 reveal intriguing temporal trends for the marker classes that characterize each cultivar; Table 2 details the LC-MS/MS data used for structural elucidation of the compounds.

For instance, Norkotah Russet extracts displayed a progression from notably abundant amino acids, phenolic acids, phenolic amines, and sterols (days 0–3); to more complex phenolic amines, sterols, glycoalkaloids and esters of fatty acids (day 7) (Fig. 7a, Table 1). Thus at early wound-healing time points the markers included amino acids (e.g., phenylalanine, tyrosine), sterols (e.g., dimethoxy-[trimethyl-(tetramethyl glucopyranosyl)-glucopyranosyl]oxy-lanost-en-one), phenolic amines (e.g., dihydroferuloylputrescine, caffeoylputrescine and feruloylputrescine) and phenolic acids (e.g., quinic acid and caffeoylquinic acid); in contrast the hallmarks of the later wound-healing stages were glycoalkaloids (e.g., Leptinine I and Solamarine), and feruloyl esters of a fatty acid (e.g. Dicaffeoyl ester of trihydroxy-6,8,10,12-eicosatetraenoic acid). No amino acid or phenolic acid markers were detected beyond day 0 and day 1, respectively. The late-stage observation of a marker which is an ester of phenolic acids and includes a hydroxyfatty acid may suggest the formation of building blocks for the suberin biopolymer. Analogously, the temporal marker variations support the formation of glycoalkaloids from sterols that has been reported independently (Ginzberg, et al., 2009).

For the Atlantic cultivar, day-0 markers included numerous phenolic amines and phenolic acids (as for Norkotah Russet) as well as significant numbers of glycoalkaloids and feruloxy fatty acids (Fig. 7b, Table 1). However, we observed a sharp drop in the number of phenolic amine and phenolic acid markers at subsequent wound-healing time points. No phenolic acid or sterol markers were detected beyond day 1, and no phenolic amines were present at day 7.

The sole Atlantic markers that persisted throughout the wound healing period were the glycoalkaloids.

Chipeta displayed a phenolic acid, an amino acid, and feruloxy fatty acids as markers at day 0; an amino acid and a glycoalkaloid marker also appeared at day 1. Moreover, this cultivar showed a gradual buildup of phenolic amine markers at later time points (Fig. 7c, Table 1). No phenolic acid markers were observed after day 0.

Finally, Yukon Gold showed several intriguing 'all-or-nothing' trends (Fig. 7d, Table 1). There were phenolic amine markers observed throughout the wound-healing process but no glycoalkaloids. Phenolic acid markers were present at the early wound-healing stages, but none were found beyond day 1.

2.4. LC-MS Metabolite Profiling: Temporal Variation of Percentage Compositions

To complement our accounting of the distinctive chemical compounds present in each potato cultivar during the course of wound healing, we also monitored shifts in the quantitative balance among structural classes within each extracted polar metabolite mixture as a function of time. Phenolic amines and glycoalkaloids were the most dominant metabolite classes for all four cultivars and at all wound-healing time points (days 0–7). Fig. 8a illustrates two striking trends for the Norkotah Russet cultivar. First, the percentage of phenolic amines holds steady from day 0 to day 3 (40.1 ± 1.1%) but decreases sharply (to 7.2%) at day 7. Concurrently, a constant percentage of glycoalkaloid metabolites is found during the temporal resistance period, whereby no significant changes are observed from day 0 to day 3 (58.9 ± 1.2%), but a marked increase (to 77.0%) occurs at day 7. Notably similar trends are observed for Atlantic, a cultivar that also exhibits skin russeting. Thus, Fig. 8b shows a slight increase in the percentage of phenolic amine content from day 0 to day 1 but again no significant changes from day 0 to day 3 (41.3 ± 1.2%) and then a significant decrease (to 16.2%) at day 7. For the Atlantic glycoalkaloids, the percentages are fairly constant through day 3 (53.3 ± 3.5%), but again a sharp increase (to 74.4%) is observed at day 7.

A rather different set of temporal variations is observed for the least russeted Chipeta and Yukon Gold cultivars. Fig. 8c shows that Chipeta exhibits a doubling of phenolic amine content from day 0 to day 1 (to 60.5%), followed by a drop below the day-0 percentage at day 2 and then modest increases to 22.2% on day 7. The trend for Chipeta glycoalkaloids is quite the opposite: a 35% drop in percentage composition from day 0 to day 1 followed by more than doubling at day 2 and steady values of ~80% thereafter. Finally, for Yukon Gold the proportion of phenolic amines stays constant at ~60% from day 0 to day 1, then drops by half at days 2 and 3 but rises substantially to 33% at day 7 (Fig. 8d). The percentage composition of glycoalkaloids remains near 38% from day 0 to day 1, then jumps up to its final values of ~65% at days 2–7.

3. Discussion

The antibacterial activity exhibited against both *E. coli* and *E. carotovora* by polar extracts from potato periderms shows a consistent decrease from early (days 0–2) to later (days 3–7)

wound-healing time points, as illustrated in Figures 2 and 3. Significantly, both the observation of robust antimicrobial activity and its diminishing magnitude occur prior to formation of the closing layer and development of wound periderm at the tissue surface (Lulai, et al., 2016; Lulai & Corsini, 1998). It is reasonable, then, to ascribe these defensive attributes to a stress response that involves a burst in the production of antibacterial metabolites, which are present during the early phase of the wound-healing process prior to the formation of a physical periderm barrier. Alternatively it is possible to invoke the presence of phytoanticipins that predispose the tubers to resist bacterial infection (VanEtten, et al., 1994). The decreasing trend in antimicrobial action over this time period could be attributed to the incorporation of these compounds into the developing suberin polymer. Alternatively, the drop-off in antibacterial activity could represent a negative feedback mechanism triggered by the formation of these metabolites. The proposed phenomenon of temporal resistance (Lulai & Corsini, 1998) that precedes tissue sealing and physical barrier initiation is also supported in molecular terms discussed below: by the identification of abundant compounds present at key time points during tuber healing and through quantitative estimation of major metabolite classes common to the four-cultivar study group.

With respect to the specific compounds that distinguish particular cultivars or wound-healing time points (Table 1), several of the amino acids, phenolic acids, phenolic amines, glycoalkaloids, sterols, flavonoids, ferulic acids, and feruloxy fatty acids stand out. Among these classes of metabolites, both phenolic acids and phenolic amines have reported antimicrobial properties that can offer protection to the wounded surface of the tuber (Back, 2001; Cueva, et al., 2010; Georgiev, et al., 2012). Thus the large numbers (and mass percentages discussed below) of phenolic amine and phenolic acid markers found in the extracts at early wound-healing time points, and the disappearance of phenolic acids by day 2, could rationalize the high antibacterial activities of the polar extracts, especially at the earliest day-0 and day-1 time points (Table 1). Moreover, the presence of numerous phenolic amine and phenolic acid markers in the day-0 Atlantic extract can explain why it is the most potent extract against the potato pathogen *E. carotovora*. For instance, common markers of wound healing observed for all cultivars include feruloylputrescine and derivatives such as dihydroferuloylputrescine. These markers are especially prevalent during early wound-healing time points in the russeted cultivars (Table 1). In Norkotah Russet and Atlantic these compounds occur as markers at day 0, whereas in other cultivars they appear at later time points (Table 1). In the same way, the bis(feruloyl)cadaverine and feruloyloctopamine marker can account for the potency of the Yukon Gold extract against *E. carotovora*. A fifth notable marker associated with early wound-healing time points is ferulic acid, identified as a day-0 marker in all cultivars with the exception of Chipeta. Our antibacterial assessments demonstrate significant antibacterial activity for both ferulic acid and feruloylputrescine (K. Dastmalchi and M. Perez Rodriguez, Personal communication), and previously published data indicate the potential of dihydroferuloylputrescine in treatments to combat the *E. carotovora* bacterium (Cueva, et al., 2010), which is a significant contributor to crop waste (van der Wolf & De Bore, 2007).

In addition to the findings of phenolic amine and phenolic acid marker compounds that help to explain the observed antibacterial activities, the time-dependent changes in biomarker structure exhibit distinctive patterns for each cultivar. Thus Norkotah Russet displays a clear

transition from simple metabolites at earlier wound-healing time points to more complex structures at later stages. For example, we find a transition from simple amines and amino acids (phenylalanine and spermine) at day 0 to phenolic amines and glycoalkaloids at later time points. The observed transition from sterol to glycoalkaloid markers for this cultivar could indicate biosynthetic incorporation of the former structures into the latter compounds along with the nitrogen contributed by an amino acid. By contrast, glycoalkaloid markers are absent at the late wound-healing points or altogether for the least russeted Chipeta and Yukon cultivars.

Turning to quantitative abundance by metabolite class in the polar tissue extracts, the phenolic amines constitute a dominant metabolite type for each cultivar until the initiation of secondary suberization at day 7. As noted above and exemplified by our independent measurements for the phenolic amines feruloylputrescine and feruloyltyramine against *E. carotovora* (K. Dastmalchi and M. Perez Rodriguez, Personal communication), these metabolites display antibacterial properties (Fewell & Roddick, 1997; Georgiev, et al., 2012). For the most heavily russeted Norkotah Russet and Atlantic cultivars, the drop-off in phenolic amine proportions occurs between day 3 and day 7, i.e., at the initiation of wound periderm formation. In the less russeted Chipeta and Yukon Gold varieties, however, the phenolic amines decrease sharply at day 2, before closing layer formation. These contrasting temporal behavior patterns of the phenolic amines align with our prior solid-state ^{13}C NMR finding of preferential polymeric suberin deposition at days 3 and 7 for the least russeted cultivars (Dastmalchi, et al., 2015). That is, the burst of antimicrobial metabolites diminishes for Chipeta and Yukon Gold cultivars just as the barrier layer is becoming established, and the reduced metabolite quantities are likely linked to their enzymatically catalyzed incorporation into the developing suberin biopolymer.

Finally, a notable observation concerns the quantitative interplay between the two most dominant classes of metabolites, phenolic amines and glycoalkaloids, which is observed consistently at all wound-healing time points and in all four cultivars (Fig. 8). In addition to the antibacterial defensive function noted above for phenolic amines, antifungal and insecticidal properties have been reported for the glycoalkaloids (Fewell & Roddick, 1997; Sanchez-Maldonado, et al., 2016). These latter compounds have been proposed to form in response to stress (Ginzberg, et al., 2009) and have been found previously in the wound tissues of potato tubers (Dastmalchi, et al., 2014). As the percentage composition of phenolic amines decreases temporally, the proportion of glycoalkaloids increases during the wound-healing process. Thus, even as the burst of antibacterial phenolic amine compounds dissipates, the already dominant glycoalkaloids “take up the slack” in the mixture composition.

4. Conclusions

This coordinated functional and molecular investigation of the early temporal course of potato tuber defense after wounding serves to demonstrate the antibacterial activities, underlying chemical contributors, and possible relationships of this phenomenon to the developing suberized cell-wall barrier. Both the generality of the temporal resistance and its cultivar-specific attributes can inform the design of practical strategies to achieve robust

plant protection and agricultural hardiness, while also identifying candidates for the molecular constituents of engineered surfaces with beneficial antimicrobial capabilities.

5. Experimental

5.1 Plant materials

Solanum tuberosum (potato) tubers from Norkotah Russet, Atlantic, Chipeta, and Yukon Gold cultivars harvested in 2015 were obtained from Dr. David Holm (Colorado State University, Fort Collins, CO).

5.2 Chemicals

LC-MS grade water and acetonitrile were purchased from J. T. Baker (Center Valley, PA), MS grade formic acid from Sigma-Aldrich (St. Louis, MO), and Analytical grade chloroform and methanol from Fisher Scientific (Pittsburgh, PA).

5.3. Sample preparation

Wound induction, isolation of wound tissues at various time points, and subsequent extractions followed the procedures described previously (Dastmalchi, et al., 2015). First, the potato tubers were peeled under aseptic conditions; a cork borer and a knife were used to section the internal tissues longitudinally into 5-mm thick disks. The disks were then placed in a dark sterile chamber controlled at 25 °C, on a shelf covered with autoclaved paper towels that was situated above a layer of autoclaved deionized water to maintain humidity. After specific time periods between 0 and 7 days after wounding, the newly developed fresh brown skin was harvested with a spatula and ground under liquid nitrogen using a mortar and pestle. Ground samples were kept frozen for at least 24 hours at −70 °C and then lyo philized.

For multiphase extraction, 2 mL of 60% (v/v) methanol-water were added to a 10-mg portion of each lyophilized sample, vortexed for about 5 s, and ultrasonicated (Branson Ultrasonics, Danbury, CT) for 1 min. A 2-mL portion of chloroform was then added to the mixture, and the process was repeated. The extracts were incubated at room temperature in a shaker for 10 min and centrifuged at 1089 g to separate three phases: soluble polar, soluble nonpolar, and a solid suspension at the interface between the two. A minimum of 1000 μL from each of the polar and nonpolar phases was extracted into clean vials, carefully avoiding cross contamination between phases. The solid suspended particles were stored at room temperature, and the polar extracts were stored at - 20 °C. The soluble nonpolar extracts were placed inside a fume hood, replacing the caps by clean aluminum foil with small punched holes to allow for overnight evaporation to dryness and then storage at −20 °C.

5.4. Antibacterial Assays

Bacterial cultures of non-pathogenic *E. coli* (Strain MG1655) and the potato pathogen *E. carotovora* (ECC15), were streaked and diluted into 2 mL of Mueller-Hinton broth, then shaken at 250 rpm and 30 °C overnight. After incubation, the cultures were diluted in Mueller-Hinton broth and normalized to achieve an optical density of 0.05 at 600 nm for subsequent antibacterial and microscopic assays, ensuring that the subsequent spectrometer

readings would not exceed a reliable range of values. Absorbance at 600 nm was used as a measure of bacterial cell viability or subsequent lysis. Using a 96-well plate, two replicate 5 mg/mL extracts from each cultivar, at each of five wound-healing time points (days 0, 1, 2, 3, and 7), were selected for testing against the two bacterial cultures together with ampicillin (positive control, well established antibacterial efficacy toward *E. coli (Thonus, et al., 1982)*) and 60% (v/v) methanol-water (negative control, the solvent in which the extracts are reconstituted). Each dried extract was reconstituted in 60% methanol to obtain a concentration of 10 mg/mL. For activity assessments, each well contained 1 μL of extracts or a control (methanol, ampicillin) and 99 μL of a bacterial culture, ensuring a reliable absorbance reading under our previously established growth conditions. The percentage inhibition for each extract was calculated as:

$$\frac{Abs(negative\ control) - Abs(sample)}{Abs(negative\ control)} \times 100$$

5.5. Microscopic Imaging

For microscopic analysis, diluted overnight cultures were combined with wound periderm extracts, ampicillin, or 60% (v/v) methanol in a ratio of 1:100 and the mixture was incubated at 30 °C for 6 hours prior to imaging. A 4-μL aliquot of each growing culture was spotted onto a pad of 2% (w/v) agarose that was premade on microscopic slides from ThermoFisher Scientific (Bridgewater, NJ). Cells were imaged using a Nikon Eclipse Ti inverted microscope with a 100x oil-immersion objective (Nikon Instruments, Melville, NY). Images were taken utilizing a DS-Qi1 monochromatic camera and processed using NIS-Elements BR 3.2 software (both from Nikon Instruments).Throughout the imaging experiments, the cells were maintained at 30 °C using a TC-500 temperature controller (20/20 Technology, Nashville, TN).

5.6. Liquid Chromatography-Mass Spectrometry (LC-ESI-MS) Analysis

The polar extracts from the potato wound tissues were analyzed using an Agilent 6550 quadrupole time-of-flight (Q-TOF) mass spectrometer (Santa Clara, CA) equipped with an Agilent 1290 Infinity high-pressure liquid chromatography (LC) system. A 2.1 mm x 50 mm, 2.7-μm reverse phase C18 column (Agilent Poroshell 120) was used with the column oven set to 30 °C and an injection volume of 20 μL. The mobile phase consisted of (A) water containing 0.1% (v/v) formic acid and (B) acetonitrile containing 0.1% (v/v) formic acid. The flow rate was 0.4 mL/min, with gradient elution conducted as follows: 0–6 min: 2% B; 6–25 min: 2–98% B; 25–27 min: 98% B; 27–30 min: 2% B. Electrospray ionization (ESI) mass spectra were acquired separately in negative and positive ion modes for the range *m/z* 100–1500. The mass spectrometer parameters were set as follows: gas temperature, 250 °C; drying gas flow, 17 L/min; nebulizer pressure, 30 psig; sheath gas temperature, 250 °C; sheath gas flow, 12 L/min; Vcap, 3500 V; nozzle voltage, 2000 V; reference masses for negative mode (112.9855, 1033.9881) and for positive mode (121.0508, 922.0097). Data were acquired and processed with Agilent's MassHunter workstation software, which includes LC/MS Data Acquisition (vB.05.01) and Qualitative Analysis (vB.06.00).

5.7. Multivariate Statistical Analysis

Simca-P+ software version 13.0 (Umetrics, Umea, Sweden) was used to carry out principal component analysis (PCA) of LC-MS data processed with MZmine, using Pareto scaling to improve detection of low-abundance ions (Worley & Powers, 2013). The PCA method organizes the data by relating the observations, sample types, and variables of the LC-MS data (retention times and *m/z* ratios of the ions), checking the consistency of each set of biological replicates and discriminating among the different sample types without *a priori* knowledge of the metabolites to be compared. The PCA plots used for analyses of LC-MS data were each validated by calculating the R^2 and Q^2 values, which indicate fitness and predictive ability, respectively (Dastmalchi, et al., 2015). The Q^2 value exceeded 0.5 in all analyses, thereby cross-validating the PCA models used. For each analysis, the R^2 value was larger than the corresponding Q^2 value (Dastmalchi, et al., 2015).

OPLS-DA analysis (Wiklund, 2008) of the data followed by the generation of S-plots helps to identify compounds that account for the differences among cultivars and between various wounding time points, respectively (Dastmalchi, et al., 2014), where a probablility threshold of 0.8 was used to assess significance (Fig. 6). OPLS-DA reveals how these two sets of information vary together and if they are dependent on each other, facilitating classification schemes and biomarker identification. As outlined previously (Dastmalchi, et al., 2015; Jin, et al., 2018), the OPLS-DA model was validated using, in addition to the Q^2 value, model diagnostics such as R^2X and R^2Y which correspond to X and Y variables (Dastmalchi, et al., 2015). The OPLS-DA results were visualized using an S-plot. The *m/z* and retention time variables at the extreme ends of the S-plot, which had probability thresholds of more than 0.8 indicating high reliability, were used to designate biomarkers (Dastmalchi, et al., 2015). A variable line plot for each selected ion was used to check how specific the biomarker was to the sample type (Wiklund, 2008). The distinguishing metabolites were identified by comparison of observed *m/z* and fragmentation patterns with published results.

Acknowledgements

The authors thank Dr. David Holm (Colorado State U.) for supplying the potato tubers. We acknowledge the gracious assistance of Dr. Anuradha Janakiraman and Mr. Aaron Mychack (CUNY City College of New York) for providing the *E. carotovora* (ECC15) and *E. coli* (MG1655) strains, equipment access, and technical assistance for the antibacterial assays. We thank Mr. Oseloka Chira for technical assistance. This work was supported by a grant from the U.S. National Science Foundation (NSF MCB-1411984 to R.E.S.); M.P.R. and J.L. were participants in Research Experiences for Undergraduates (REU) and Research Assistantships for High School Students programs, respectively, under this grant award. Additionally, the work was underwritten by fellowships to M.P.R. in an NIH Research Initiative for Minority Students Bridges to the Baccalaureate Program linking Queensborough Community College and CCNY (NIH 5R25GM065096–16); an NSF REU site in Biochemistry, Biophysics, and Biodesign at CCNY (NSF DBI-1560384), the NYC Louis Stokes Alliance for Minority Participation CUNY (NSF HRD-1202520); an NIH Maximizing Access to Research Careers Program at CCNY (NIH 5T34GM007639–37), and a City College Fellowship. The Q-TOF MS instrument was acquired through NSF award CHE-1228921 and is operated by the CUNY Hunter College Department of Chemistry and Biochemistry. Infrastructural support was provided by The City College of New York, the CUNY Institute for Macromolecular Assemblies, and a grant from the U.S. National Institutes of Health (5G12MD007603–30, National Institute on Minority Health and Health Disparities).

References Cited

Back K 2001 Hydroxycinnamic acid amides and their possible utilization for enhancing agronomic traits. Plant Physiol, 17, 123–127.

Bartke N, Fischbeck A, & Humpf H-U 2006 Analysis of sphingolipids in potatoes (Solanum tuberosum L.) and sweet potatoes (Ipomoea batatas (L.) Lam.) by reverse phase high-performance liquid chromatography electrospray ionization tandem mass spectrometery (HPLC-ESI-MS/MS). Mol. Nutr. Food Res, 50, 1201–1211. [PubMed: 17103377]

Cruz CD, Fletcher GC, & Pajak MA 2014 Tannins and extracts of fruit byproducts: Antibacterial activity against foodborne bacteria and antioxidant capacity. J Agric. Food Chem, 62, 11146–11156. [PubMed: 25339414]

Cueva C, Moreno-Arribas MV, Martin-Alvarez PJ, Bills G, Vicente MF, Basilio A, Rivas CL, Requena T, Rodriguez JM, & Bartolome B 2010Antimicrobial activity of phenolic acids against commensal, probiotic and pathogenic bacteria. Res. Microbiol, 161, 372–382. [PubMed: 20451604]

Czajkowski R, Perombelon MCM, van Veen JA, & van der Wolf JM 2011 Control of blackleg and tuber soft rot of potato caused by Pectobacterium and Dickeya species: a review. Plant Pathol, 60, 999–1184.

Dastmalchi K, Cai Q, Zhou K, Huang W, Serra O, & Stark RE 2014 Solving the Jigsaw puzzle of wound-healing potato cultivars: Metabolite profiling and antioxidant activity of polar extracts. J. Agric. Food Chem, 62, 7963–7975. [PubMed: 24998264]

Dastmalchi K, Kallash L, Wang I, Phan VC, Huang W, Serra O, & Stark RE 2015 Defensive armor of potato tubers: Nonpolar metabolite profiling, antioxidant assessment, and solid-state NMR compositional analysis of suberin-enriched wound-healing tissues. J. Agric. Food Chem, 63, 6810–6822. [PubMed: 26166447]

Dastmalchi K, Wang I, & Stark RE 2016 Potato wound-healing tissues: A rich source of natural antioxidant molecules for food preservation. Food Chem, 210, 473–480. [PubMed: 27211673]

des Essarts YR, Cigna J, Quetu-Laurent A, Caron A, Munier E, Beury-Cirou A, Helias V, & Faure D 2016 Biocontrol of the potato blackleg and soft rot diseases caused by Dickeya dianthicola. Appl. Environ. Microbiol, 82, 268–278. [PubMed: 26497457]

Fewell AM, & Roddick JG 1997 Potato glycoalkaloid impariment of fungal development. Mycol. Res, 101, 597–603.

Georgiev L, Chochkova M, Ivanova G, Najdenski H, Ninova M, & Milkova T 2012 Radical scavenging and antimicrobial activities of cinnamoyl amides of biogenic monoamines. Riv. Ital. Sostanze Gr, 39, 91–102.

Ginzberg I, Tokuhisa JG, & Veilleux RE 2009 Potato steroidal glycoalkaloids: Biosynthesis and genetic manipulation. Potato Res, 52, 1–15.

Huang W, Serra O, Dastmalchi K, Liqing J, Yang L, & Stark RE 2017 Comprehensive MS and Solid-State NMR metabolite profiling reveals molecular variations in native periderms from four Solanum tuberosum potato cultivars. J. Agric. Food Chem, 65, 2258–2274. [PubMed: 28215068]

Jin L, Cai Q, Huang W, Dastmalchi K, Rigau J, Molinas M, Figueras M, Serra O, & Stark RE 2018 Potato native and wound periderms are differently affected by downregualtion of FHT, a suberin feruloyl transferase. Phytochemistry, 147, 30–48. [PubMed: 29288888]

King RR, & Calhoun LA 2005 Characterization of cross-linked hydroxycinnamic acid amides isolated from potato common scab lesions. Phytochemistry, 66, 2468–2473. [PubMed: 16137726]

Landgraf R, Smolka U, Altmann S, Eschen-Lippold L, Senning M, Sonnewald S, Weigel B, Frolova N, Strehmel N, Hause G, Scheel D, Bottcher C, & Rosahl S 2014 The ABC transporter ABGCG1 is required for suberin formation in potato tuber periderm. Plant Cell, 26, 3403–3415. [PubMed: 25122151]

Leubner-Metzger G, & Nikolaus A 1993 The distibution of hydroxycinnamoylputrescines in different organs of Solanum tuberosum and other solanaceous species. Phytochemistry, 32(3), 551–556.

Lopatriello A, Previtera R, Pace S, Werner M, Rubino L, Werz O, Taglialatela-Scafati O, & Forino M 2017 NMR-based identification of the major bioactive molecules from an Italian cultivar of Lycium barbarum. Phytochemistry, 144, 52–57. [PubMed: 28888145]

Lulai EC (2007). Wound Healing. In Verugdenhil H (Ed.), Potato Biology and Biotechnology: Advances and Prespectives First ed., (pp. 472–500): Elsevier,The Netherlands.

Lulai EC, Campbell LG, Fugate KK, & McCue KF 2016 Biological differences that distinguish the 2 major stages of wound healing in potato tubers. Plant Signal Behav, 11(12), e31256531.

Lulai EC, & Corsini DL 1998 Differential deposition of suberin phenolic and aliphatic domains and their role in resistance to infection during potato tuber (Solanum tuberosum) wound healing. Physiol. Mol. Plant Pathol, 53, 209–222.

Lulai EC, Neubauer JD, Olson LL, & Suttle JC 2015 Wounding induces changes in tuber polyamine content, polyamine metabolic gene expression, and enzyme activity during closing layer formation and initiation of wound periderm formation. J Plant Phys, 176, 89–95.

Martin-Tanguy J, Cabanne F, Perdrizet E, & Martin C 1978 The distibution of hydroxycinnamic acid amides in flowering plants. Phytochemistry, 117(11), 1927–1928.

Martin-Tanguy J, Deshayes A, Predrizet E, & Martin C 1979 Hydroxycinnamic acid amides (HCA) in Zea mays. Distribution and changes in cytoplasmic male sterility. FEBS Letters, 108, 176–178.

Ricker KE, & Bostock RM 1994 Eicosanoids in the Phytophthora infestans-potato interaction: Lipoxygenase metabolism of arachidonic acid and biological activities of selected lipoxygenase products. Physiol. Mol. Plant Pathol, 44, 65–80.

Sanchez-Maldonado AF, Schieber A, & Ganzel MG 2016 Antifungal activity of secondary plant metabolites from potatoes (Solanum tuberosum L.): Glycoalklaoids and phenolic acids show synergistic effects. J. Appl. Microbiol, 120, 955–965. [PubMed: 26786886]

Schieber A, & Saldana MDA 2008 Potato peels: A source of nutritionally and pharmacologically interesting compounds-A review. Food 3, 23–29.

Shakya R, & Navaree DA 2008 LC-MS analysis of solanidane glycoalkaloid diversity among tubers of four wild potato species and three cultivars (Solanum tuberosum). J. Agric. Food Chem, 56, 6949–6958. [PubMed: 18616273]

Thonus IP, Fontijne P, & Michel MF 1982 Ampicillin susceptibility and ampicillin-induced killing rate of Escherichia coli. Antimicrob. Agents Chemother, 22, 386–390. [PubMed: 6753736]

Toth IK, Bell KS, Holeva MC, & Birch PRJ 2003 Soft rot erwiniae: from genes to genome. Mol. Plant Pathol, 4, 17–30. [PubMed: 20569359]

Van der Wolf JM, & De Bore SH (2007). Bacterial Pathogens of Potato. In Verugdenhil H (Ed.), Potato Biology and Biotechnology: Advances and Prespectives, (pp. 595–614): Elsevier, The Netherlands.

VanEtten HD, Mansfield JW, Bailey JA, & Framer EE 1994 Two classes of plant antibiotics: Phytoalexins versus “Phytoanticipins”. Plant Cell, 6(9), 1191–1192. [PubMed: 12244269]

Voynikonv Y, Zheleva-Dimitrova D, Gevrenova R, Lozanov V, Zaharieva MM, Tsvetkova I, Najdenski H, Yagi S, Almoulah NF, & Momekov G 2016 Hydroxycinnamic acid amide profile of Solanum schimperianum Hochst by UPLC-HRMS. Int. J. Mass Spectrom, 408, 42–50.

Wiklund S (2008). Multivariate Data Analysis and Modelling in “Omics”. In Umetrics (Ed.)): Umetrics AB.

Worley B, & Powers R 2013 Multivariate analysis in metabolomics. Curr. Metabol, 1, 92–107.

Yang WL, & Bernards MA 2007 Metabolite profiling of potato (Solanum tuberosum L.) tubers during wound-induced suberization. Metabolomics, 3, 147–159.

Highlights

1. Polar extracts from potato wound tissues showed antibacterial activity.
2. Temporal resistance was confirmed by high activity of 0–2 day old wound tissue extracts.
3. Phenolic amines and glycoalkaloids were the dominant metabolite classes.
4. Increasing glycoalkaloid and decreasing phenolic amine proportions accompanied healing.
5. Metabolite profile changes were distinctive for cultivars with contrasting skin russeting.

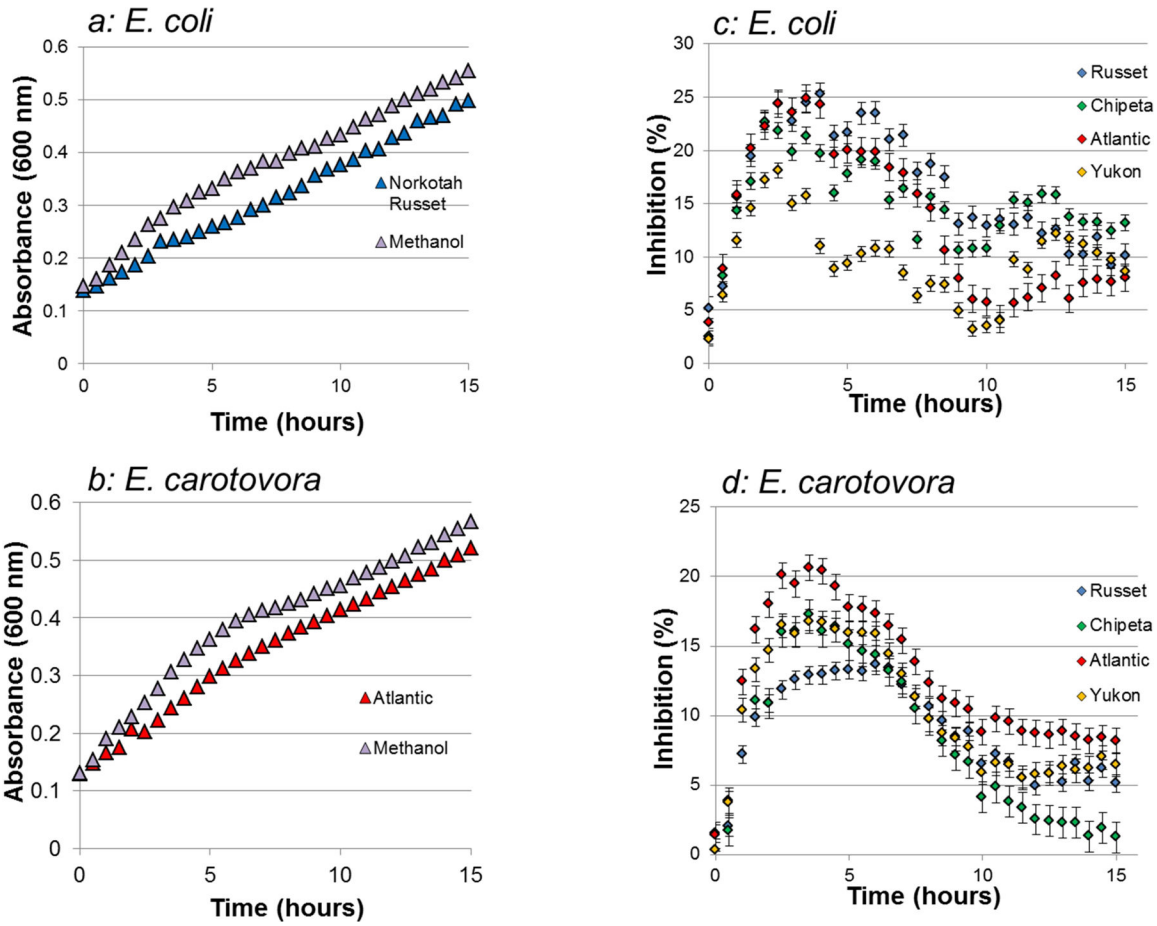

Fig.1.

Polar extracts from potato tuber wound periderms inhibit the growth of two Gram negative bacterial organisms. The effects of *Escherichia coli* and *Erwinia carotovora* exposure to polar extracts at the day-0 wound-healing time point are shown for four cultivars with differing degrees of russeting. a: Light absorbance at 600 nm for *E. coli* exposed to Norkotah Russet and a methanol control during a 15-hour experiment. b: Light absorbance at 600 nm for *E. carotovora* exposed to Atlantic and a methanol control during a 15-hour experiment. c: Percentage of growth inhibition for day-0 wound-healing polar extracts against *E. coli,* based on optical density readings. d: Percentage of growth inhibition for day-0 wound-healing polar extracts against *E. carotovora,* based on optical density readings. Both types of graphs use the same color scheme: Yukon Gold (gold), Atlantic (red), Chipeta (green), Norkotah Russet (blue), and Control (gray). Analogous plots were obtained for each of the time points after wounding (1, 2, 3 and 7; data not shown). Error bars indicate standard error from the two biological replicates per cultivar.

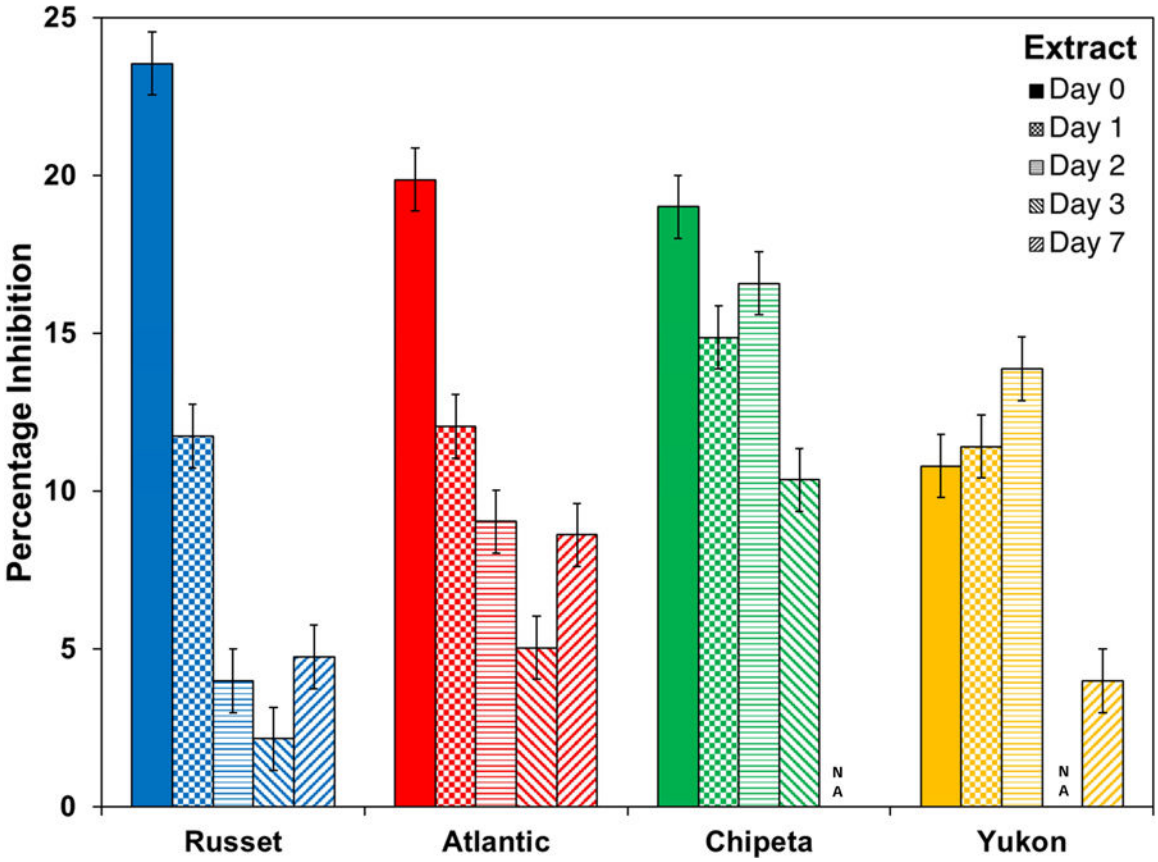

Fig. 2.

Antimicrobial activity against *E. coli* cultures at 6 hours of exposure drops off for most *S. tuberosum* polar extracts at late wound-healing time points. The bar chart uses the color scheme of Figure 1: Yukon Gold (gold), Atlantic (red), Chipeta (green), and Norkotah Russet (blue). Error bars indicate standard error from the two biological replicates per cultivar. NA: not active.

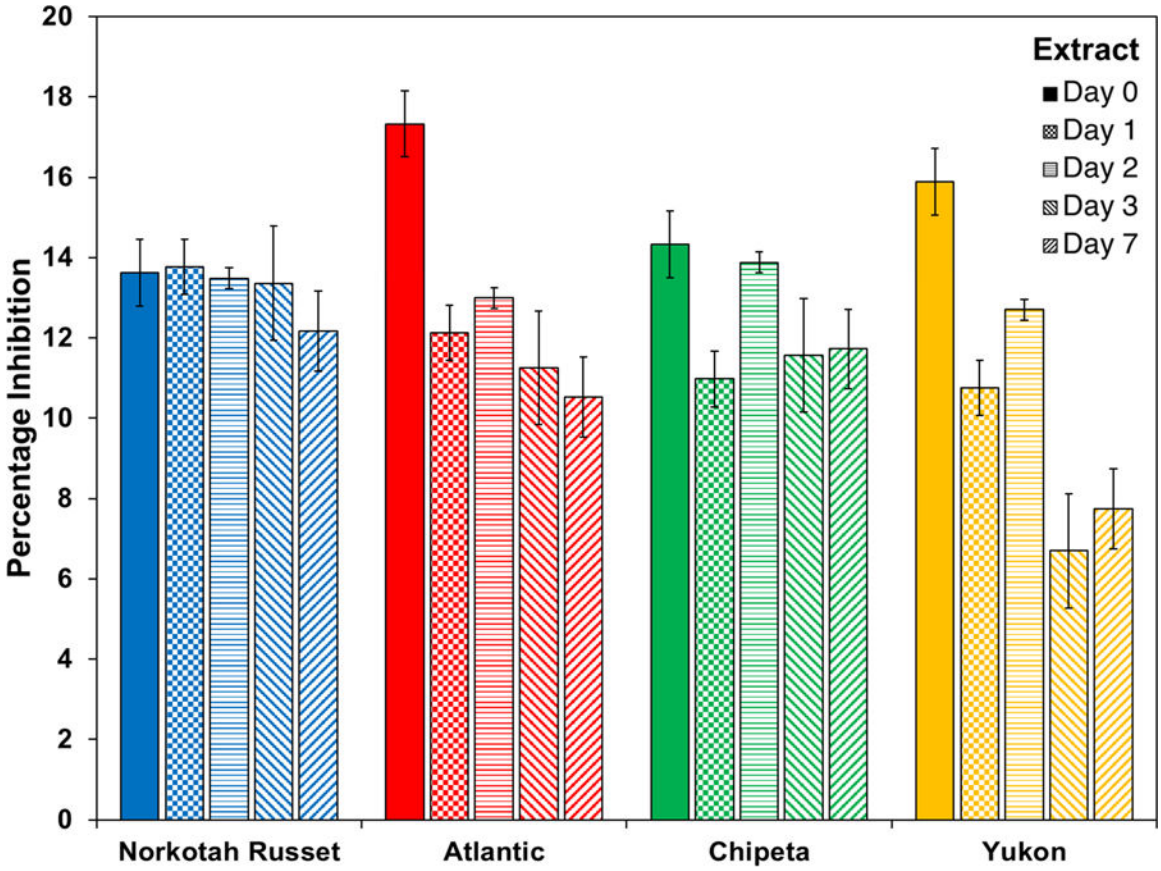

Fig. 3.

Antimicrobial activity against *E. carotovora* cultures at 6 hours of exposure drops off for all *S. tuberosum* polar extracts at late wound-healing time points. The bar chart uses the color scheme of Figure 1: Yukon Gold (gold), Atlantic (red), Chipeta (green), and Norkotah Russet (blue). Error bars indicate standard error mean from the two biological replicates per cultivar. NA: not active.

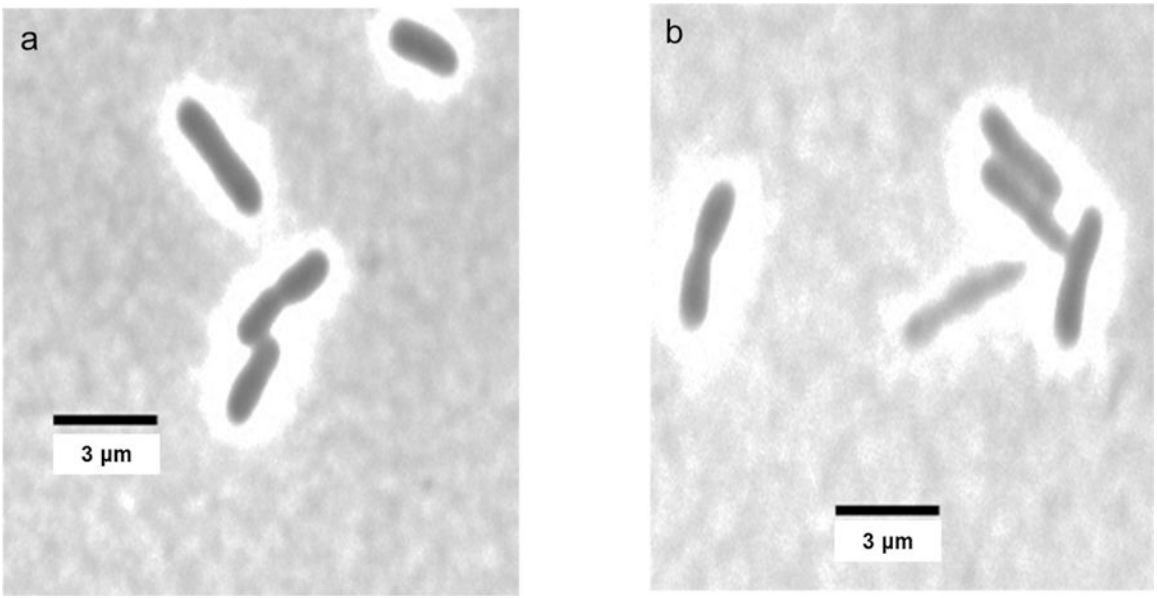

Fig. 4.

Microscopic images of *E. coli* cultures incubated with polar day-0 Norkotah Russet (Wd0R) wound periderm extracts at two concentrations. a: 8 µg/mL; b: 80 µg/mL. Cell lysis and morphological changes are observed at the higher concentration.

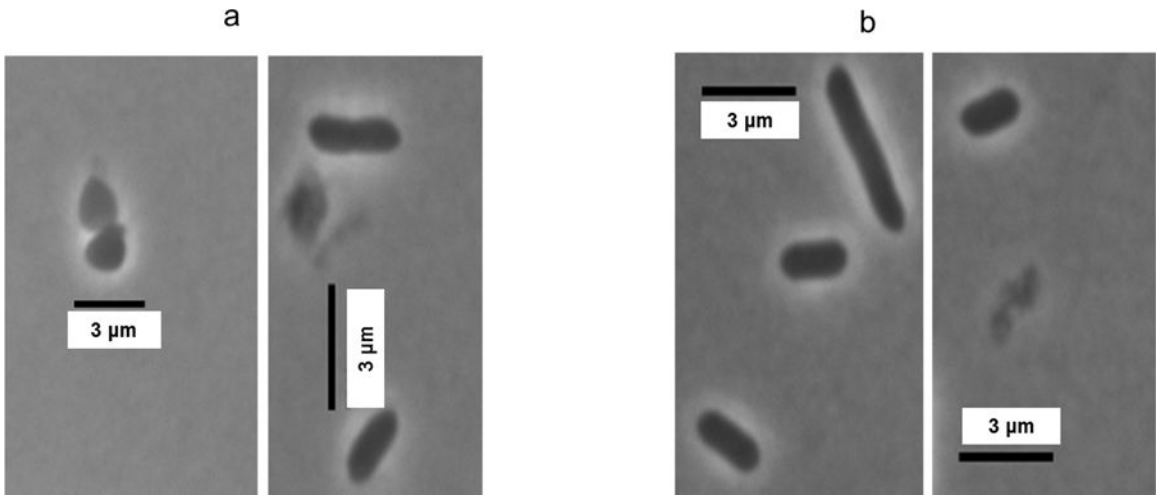

Fig. 5.

Microscopic images of *E. carotovora* cultures incubated with polar day-0 Atlantic (Wd0A) wound periderm extracts. a: 8 µg/mL; b: 80 µg/mL. Morphological changes and increased cell lysis are observed at the higher concentrations.

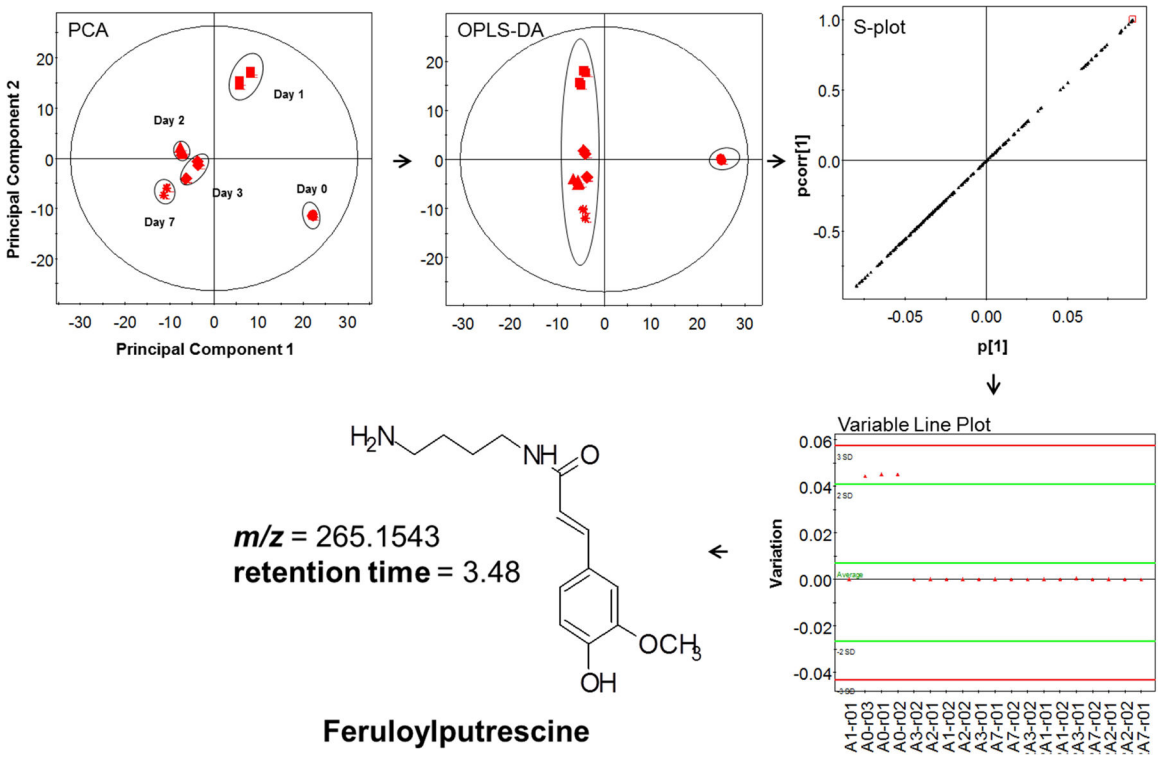

Fig. 6.

Schematic representation of multivariate statistical analysis including principal component analysis (PCA), orthogonal partial least squares-discriminate analysis (OPLS-DA), S-plot and variable line plots of LC-MS data for polar extracts of the Atlantic cultivar (red color code) obtained at different wound-healing time points: days 0, 1, 2, 3, and 7.

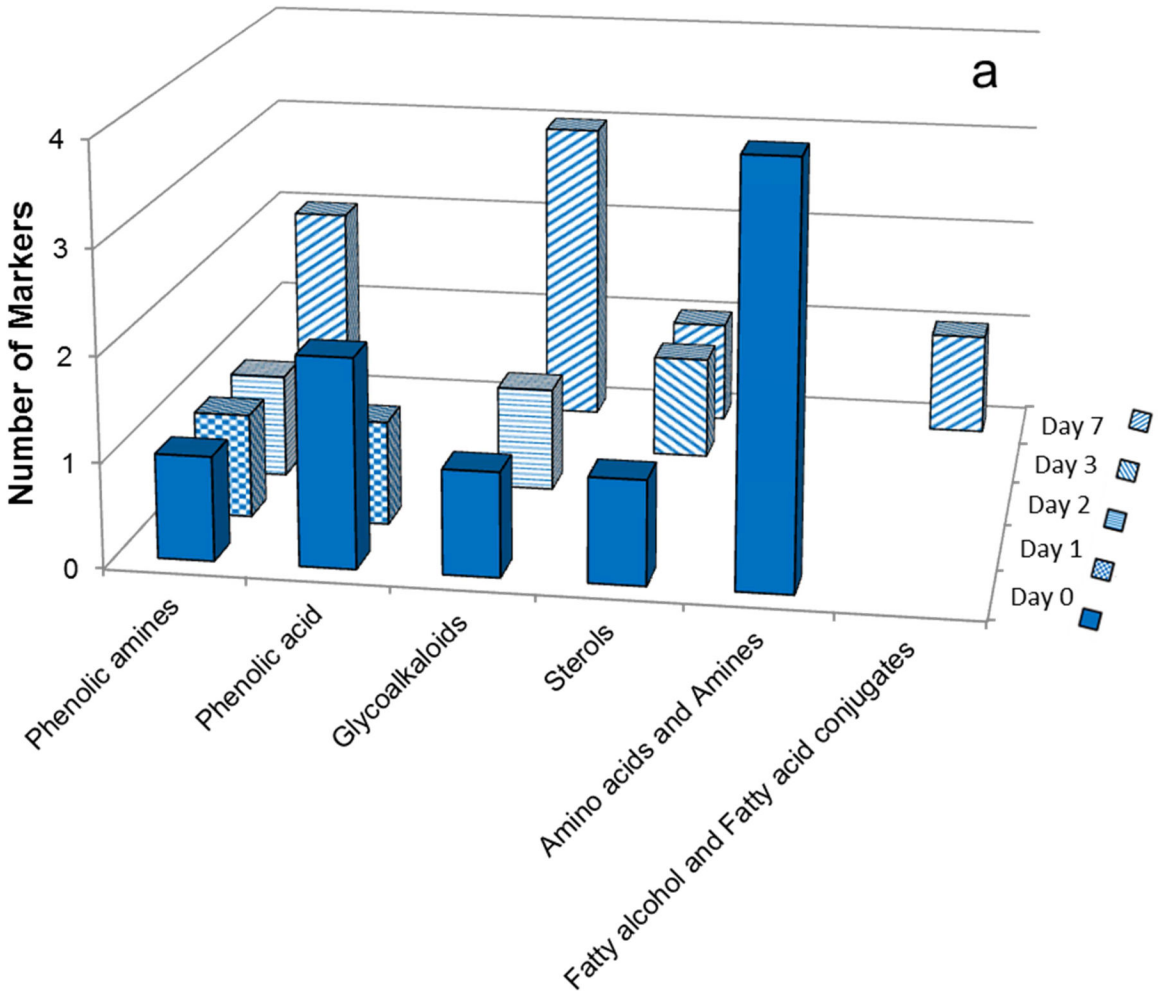

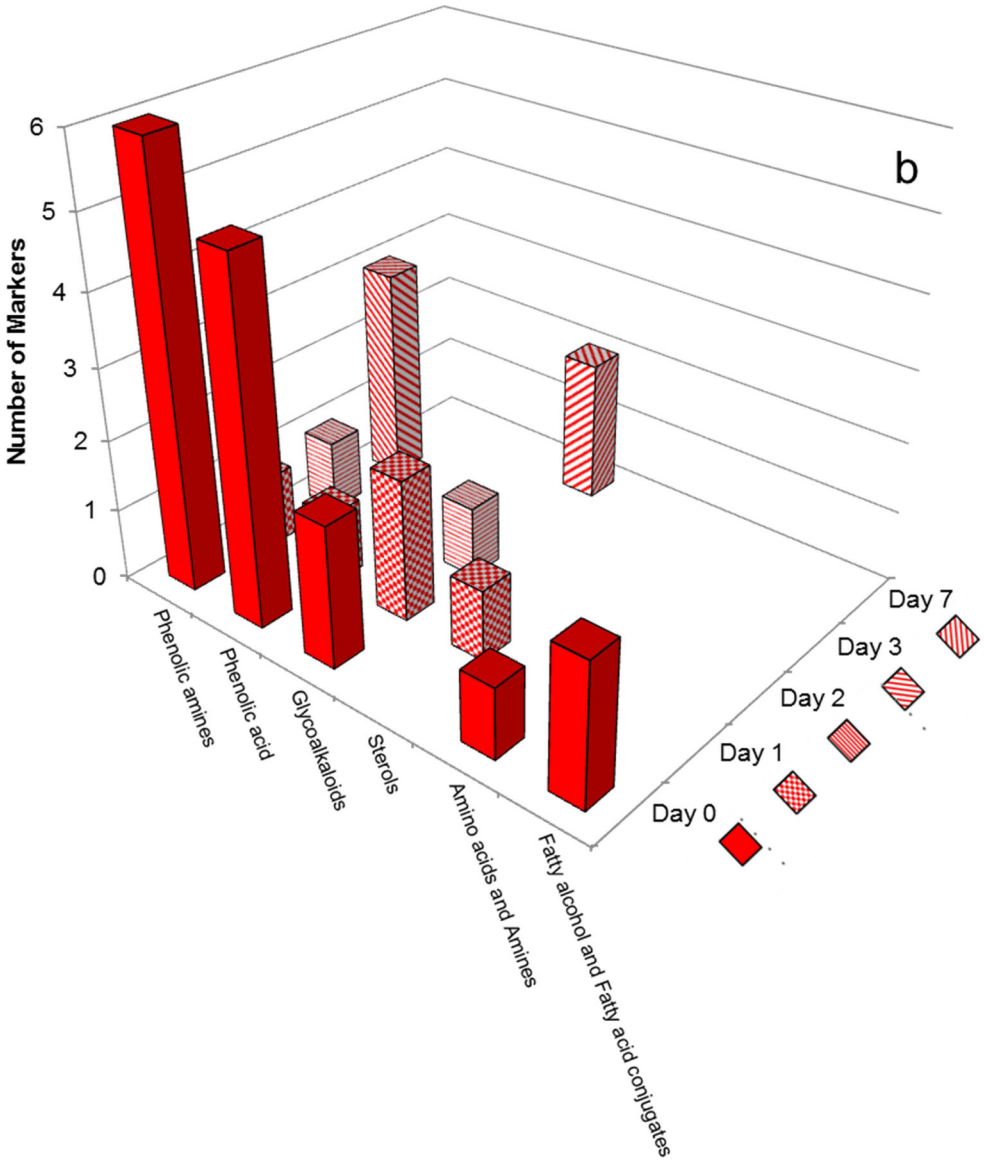

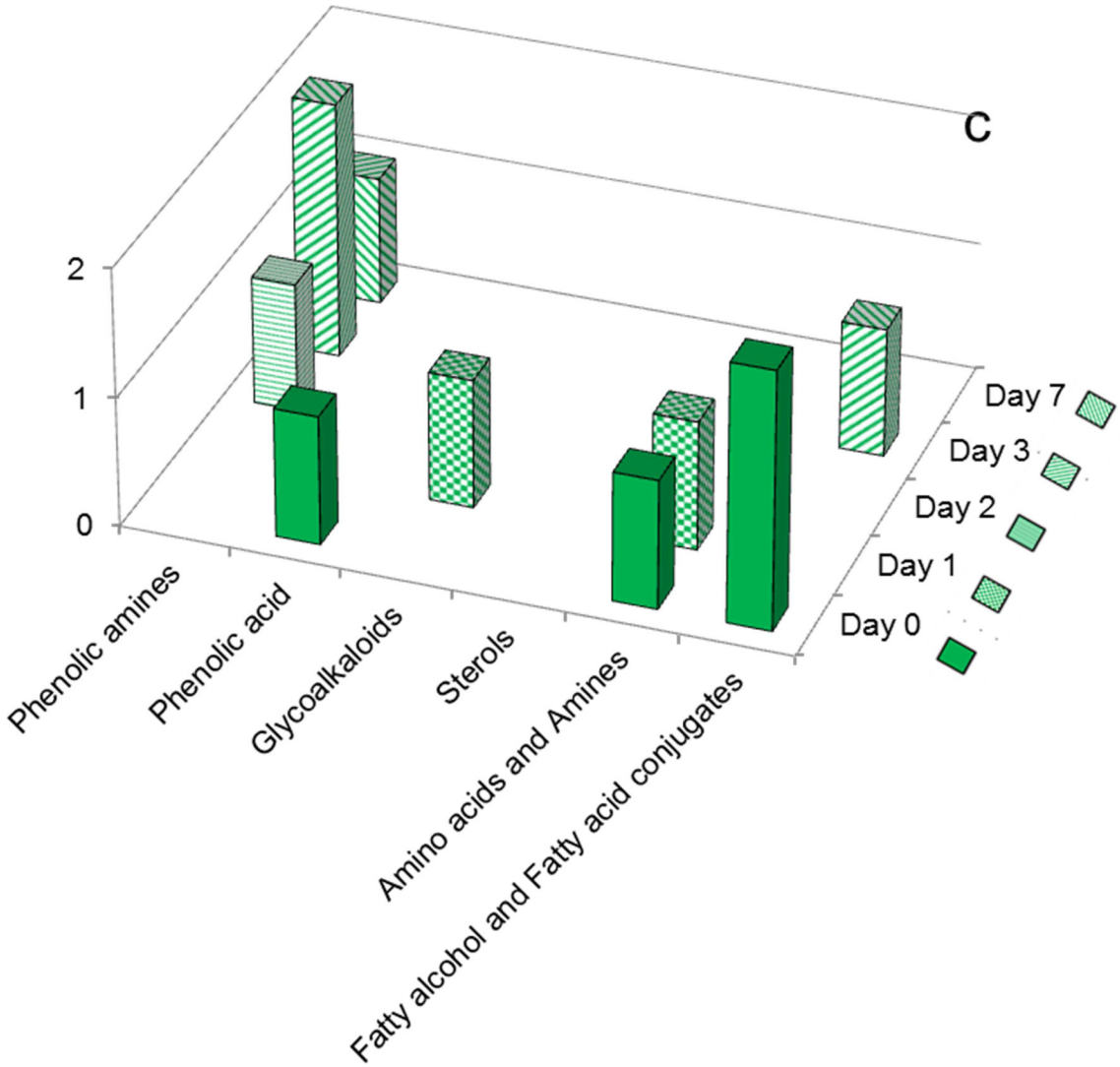

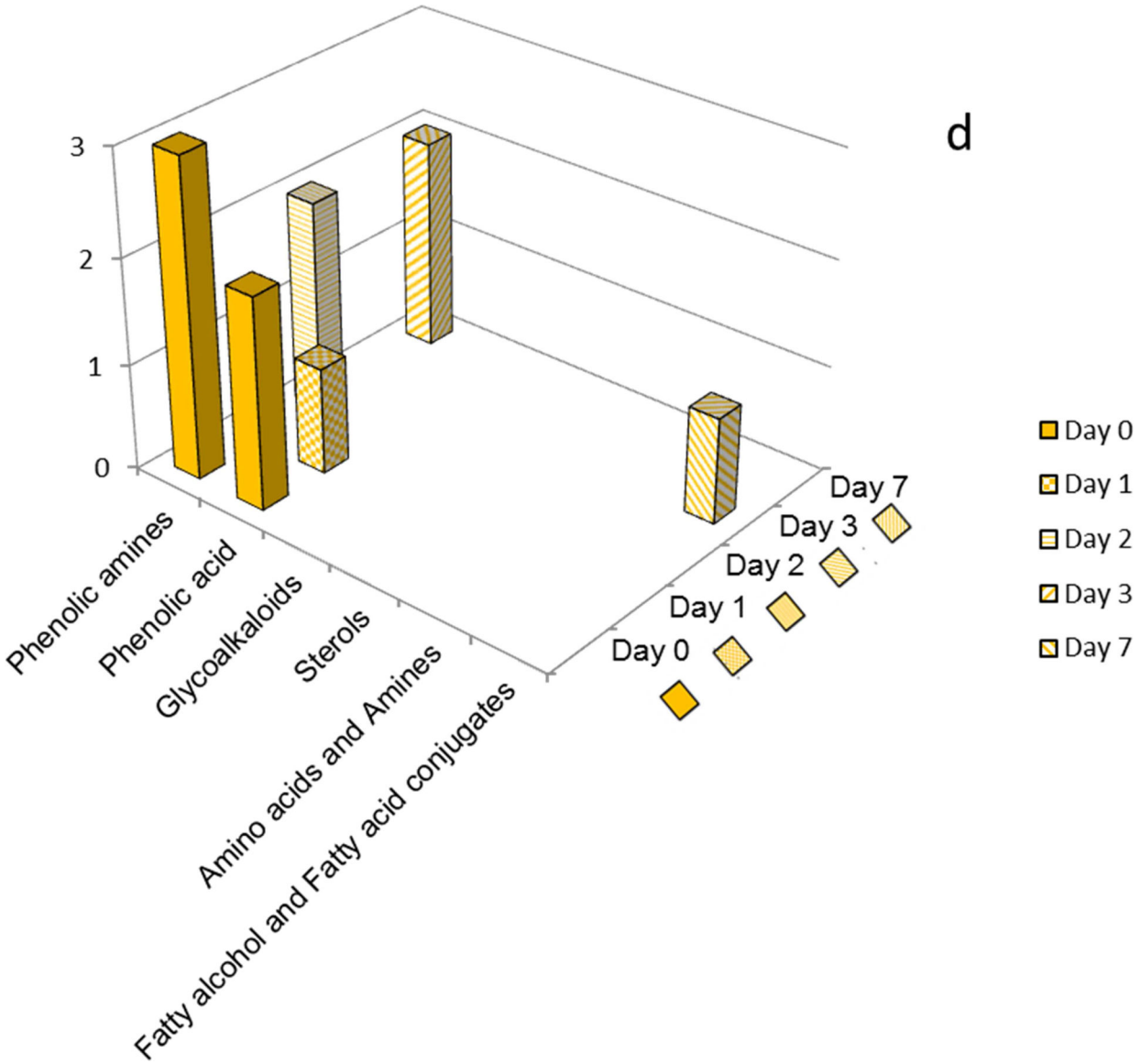

Fig. 7.

Distribution of marker compounds at several time points during the wound healing process. a: Norkotah Russet b: Atlantic c: Chipeta d: Yukon Gold. The bar chart uses the color scheme of Figure 1: Yukon Gold (gold), Atlantic (red), Chipeta (green), and Norkotah Russet (blue).

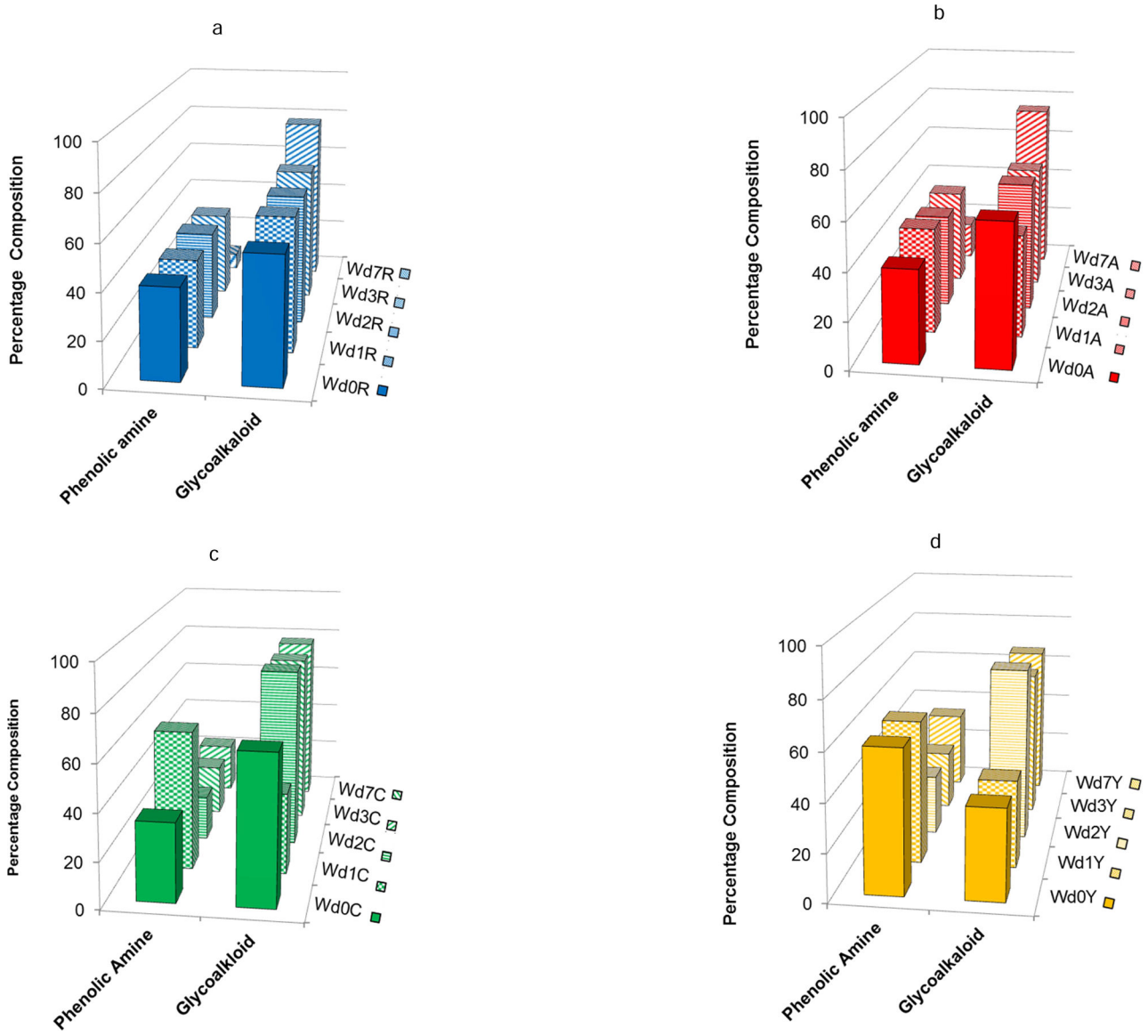

Fig. 8.

Variation in percentage composition of major metabolite classes as a function of time point during the wound healing process. a: Norkotah Russet; b: Atlantic; c: Chipeta; d: Yukon Gold. The bar chart uses the color scheme of Figure 1: Yukon Gold (gold), Atlantic (red), Chipeta (green), and Norkotah Russet (blue).

Table 1.

Potential polar marker compounds by cultivar and wound-healing time point

	Day 0	Day 1	Day2	Day 3	Day 7
Norkotah Russet	Spermine	Caffeoylquinic acid	Feruloyl putrescine	Dihydro-ASP-II	Dihydro-ASP-II
	Quinic acid		Leptinine II		
	Tyrosine	Caffeoylputrescine			Dicoumaroyl putrescine
	Phenylalanine				Feruloylputrescine isomer
	Ferulic acid				Solamarine
	Dihydroferuloylputrescine				Solanidadienol chacotriose
	α-Chaconine				Leptinine I
	Dimethoxy-[trimethyl-(tetramethylglucopyranosyl)-glucopyranosyl]oxy]-lanost-en-one				Dicaffeoyl ester of trihydroxy-Eicosatetraenoic acid
Atlantic	Phenylalanine	Coumaroylquinic acid	Leptinine II	Triferuloyl putrescine	Solamarine
	Quinic acid	Leptinine I	Bisferuloylcadaverine	Feruloyl putrescine Isomer	Leptinine II isomer
	Ferulic acid	Dehydrocommersonine			
	Caffeoylquinic acid	Protodioscine		Feruloylputrescine	
	Coumaroylquinic acid	Tetra(dihydrocaffeoyl)-spermine			
	Feruloylquinic acid				
	Coumaroyl putrescine				
	Dihydroferuloylputrescine				
	Feruloylputrescine				
	Caffoyldihydrocaffeoylspermine				
	Feruloyloctopamine				
	α-Solanine				
	α-Chaconine				
	Grossamide				
	Alkyl ferulate (C22:0)				
	Hydroxy alkyl (C21:0) ferulate				
Chipeta	Quinic acid	Tyrosine	Feruloylagmatin	Feruloylputrescine	Feruloylacetylputrescine
	Phenylalanine	α-Solanine		Feruloylcadaverine	
	Dicaffeoyl ester of trihydroxy-eicosapentaenoic acid			2-amino-, −1,3,4-triol, 8-Octadecene	
	Dicaffeoyl ester of trihydroxy-Eicosatetraenoic acid				
Yukon Gold	Ferulic acid	Caffeoylquinic acid	Caffeoyl-dihydrocaffeoyl-spermine	Dicaffeoyl ester of trihydroxy-Eicosatetraenoic acid	Dihydroferuloylputrescine
	Feruloyloctopamine				
	Sinapoyl putrescine		Feruloylputrescine		Feruloylacetylputrescine

	Day 0	Day 1	Day2	Day 3	Day 7
Piceatannol					
Bis-feruloylcadaverine					

Table 2.

LC-MS characterization of potential polar marker compounds from four cultivars at different wound-healing time points

Compou nd No.[a]	$[M+H]^+/[M-H]^-$ or $[M+Na]^+$	MS/MS Fragment ions (Positive)	Biomarker Formula and Molecular Weight	Structural Formula	Wound Time Point Specific Marker	References
Simple amines						
1	203.2205 $[M+H]^+$ C10H27N_4 (−12.3 ppm)		**Spermine** $C_{10}H_{26}N_4$ 202.2152	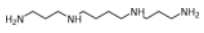	**Norkotah Russet (Wd0)**	(Yang & Bernards, 2007)
Amino acids						
2	182.0791 $[M+H]^+$ $C_9H_{11}NO_3$ (−12.6 ppm)	166	**Tyrosine** $C_9H_{11}NO_3$ 181.0733	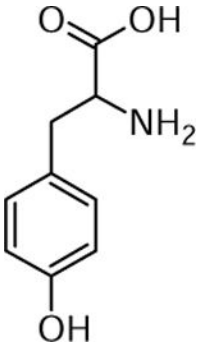	**Norkotah Russet (Wd0) and Chipeta (Wd1)**	(Yang & Bernards, 2007)
3	166.086 $[M+H]^+$ $C_9H_{12}NO_2$ (2.4 ppm)	120	**Phenylalanine** $C_9H_{11}NO_2$ 165.0784	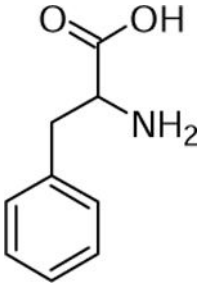	**Norkotah Russet (Wd0) and Chipeta (Wd0)**	(Yang & Bernards, 2007)
Phenolic amines						

Compou nd No.[a]	$[M+H]^+/[M-H]^-$ or $[M+Na]^+$	MS/MS Fragment ions (Positive)	Biomarker Formula and Molecular Weight	Structural Formula	Wound Time Point Specific Marker	References
4	265.1543 $[M+H]^+$ $C_{14}H_{21}N2O4$ (1.5 ppm)	177, 145, 134, 117	**Feruloyl-putrescine** $C_{14}H_{20}N_2O_3$ 264.1474	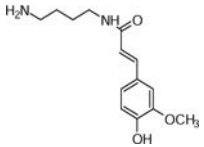	**Atlantic (Wd0), Nokotah Russet (Wd2), Chipeta (Wd3) and Yukon Gold (Wd7)**	(Dastmalchi, et al., 2014; Huang, et al., 2017)
5	265.1553 $C_{14}H_{21}N_2O_4$ (2.2 ppm)	177, 145, 134, 117	**Feruloyl-putrescine isomer** $C_{14}H_{20}N_2O_3$ 264.1474	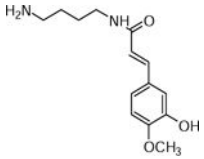	**Atlantic (Wd3) and Norkotah Russet (Wd7)**	(Dastmalchi, et al., 2014; Huang, et al., 2017)
6	267.1709 $C_{14}H_{21}N_2O_4$(2.25 ppm)	249, 221, 192, 136, 118	**Dihydroferuloyl-putrescine** $C_{14}H_{22}N_2O_3$ 266.1625	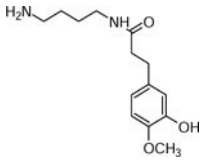	**Norkotah Russet (Wd0) Atlantic (Wd0), and Yukon Gold (Wd7)**	(Huang, et al., 2017)
7	617.2337 $C_{34}H_{37}N_2O_9$ (−25 ppm)	425, 359, 311, 265, 177	**Triferuloyl-putrescine** $C_{34}H_{36}N_2O_9$ 616.2415	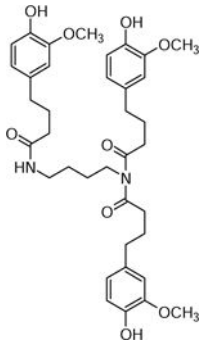	**Atlantic (Wd3) and Chipeta (Wd3)**	(Leubner-Metzger & Nikolaus, 1993)
8	295.1655 $[M+H]^+$ $C_{15}H_{23}N_2O_4$ (1.0 ppm)	280, 211	**Sinapoyl-putrescine** $C_{15}H_{22}N_2O_4$ 294.1574	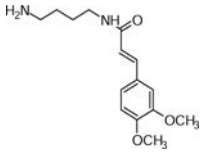	**Yukon Gold (Wd0)**	(Martin-Tanguy, et al., 1978)

Compou nd No.[a]	$[M+H]^+/[M-H]^-$ or $[M+Na]^+$	MS/MS Fragment ions (Positive)	Biomarker Formula and Molecular Weight	Structural Formula	Wound Time Point Specific Marker	References
9	251.1398 $[M+H]^+$ ($C_{13}H_{19}N_2O_3$(0.8 ppm)	179, 163, 137, 121	**Caffeoyl-putrescine** $C_{13}H18N2O3$ 250.1317	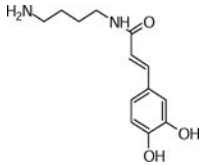	**Norkotah Russet (Wd1)**	(Dastmalchi, et al., 2014; Leubner-Metzger & Nikolaus, 1993)
10	235.1471 $[M+H]^+$ ($C_{13}H_{19}N_2O_2$ 10.2 ppm)	179, 135, 121	**Coumaryl-putrescine** $C_{13}H_{18}N_2O_2$ 234.1363	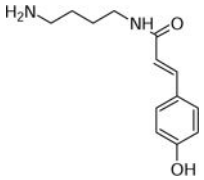	**Atlantic (Wd0)**	(Dastmalchi, et al., 2014; Leubner-Metzger & Nikolaus, 1993)
11	381.0797 $[M+H]^+$ $C_{22}H_{25}N_2O_4$ (0.4 ppm)	365, 208, 192,175	**Dicoumaroyl-putrescine** $C_{22}H_{24}N_2O_4$ 380.1731	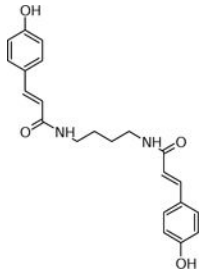	**Norkotah Russet (Wd7)**	(Jin, et al., 2018)
12	329.1473 $[M+Na]^+$ $C_{22}H_{22}N_2O_4Na$ (−0.3 ppm)	273, 185	**Feruloyl-Acetyl-putrescine** $C_{16}H_{22}N_2O_4$ 306.158	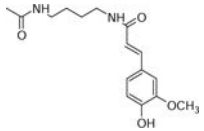	**Yukon Gold (Wd7) Chipeta (Wd7),** and **Atlantic (Wd0)**	(Lopatriello, et al., 2017)
13	307.1764 $[M+H]^+$ $C_{15}H_{23}N_4O_3$ (−0.3 ppm)	207, 195, 177	**Feruloylagmatin** $C_{15}H_{22}N_4O_3$ 306.1686	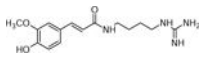	**Chipeta (Wd2)**	(Voynikonv, et al., 2016)

Compou nd No.[a]	[M+H]$^+$/[M-H]$^-$or [M+Na] $^+$	MS/MS Fragment ions (Positive)	Biomarker Formula and Molecular Weight	Structural Formula	Wound Time Point Specific Marker	References
14	657.2432 [2M+H]$^+$ $C_{36}H_{37}N_2O_{10}$ (1.67 ppm)	315, 294, 209	**Feruloyl-octopamine** C18H19NO5 329.1258	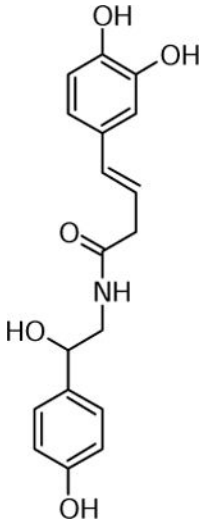	**Yukon Gold (Wd0)**	(King & Calhoun, 2005)
15	279.1708 $C_{18}H_{20}NO_4$ (−1.73 ppm)	239, 177	**Feruloyl-cadaverine** $C_{15}H_{22}N_2O_3$ 278.1625	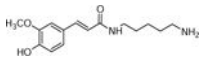	**Chipeta (Wd3)**	(Voynikonv, et al., 2016)
16	455.2416 $C_{18}H_{20}NO_4$ (−5.5 ppm)	246, 195	**Bis-feruloyl-cadaverine** C22H30N2O6 454.2098		**Atlantic (Wd2) and Yukon (Wd0)**	(Martin-Tanguy, et al., 1979; Voynikonv, et al., 2016)
17	529.3008 [M+H]$^+$ $C_{28}H_{40}N_4O_6$ (−2.4 ppm)	365, 345, 319, 309	***N,N*-bis (caffeoyldihydro-caffeoyl) spermine** $C_{28}H_{39}N_4O_6$ 528.2942	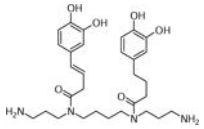	**Atlantic (Wd0) and Yukon gold (Wd2)**	(Dastmalchi, et al., 2014)
18	881.3691 [M+Na]$^+$ $C_{46}H_{58}N_4O_{12}Na$ (−30.82 ppm)	677, 547, 365, 345, 319, 309	**Tetra (dihydrocaffeoyl) spermine** $C_{46}H_{58}N_4O_{12}$ 858.4046	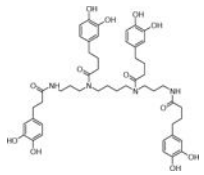	**Atlantic (Wd1)**	(Dastmalchi, et al., 2014)

Compou nd No.[a]	$[M+H]^+/[M-H]^-$ or $[M+Na]^+$	MS/MS Fragment ions (Positive)	Biomarker Formula and Molecular Weight	Structural Formula	Wound Time Point Specific Marker	References
19	625.2567 $[M+H]^+$ $C_{36}H_{37}N_2O_8$ (2.87ppm)	369, 211, 116	**Grossamide** $C_{36}H_{36}N_2O_8$ 624.2471	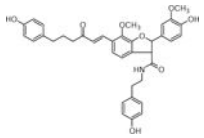	**Atlantic (Wd0)**	(Dastmalchi, et al., 2014)
Phenolic acids						
20	215.0592 $C_7H_{12}O_6Na$ $[M+Na]^+$ (2.2 ppm)	175,112	**Quinic acid** $C_7H_{12}O_6$ 192.0634	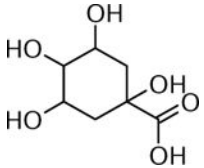	**Norkotah Russet (Wd0), Atlantic (Wd0) and Chipeta (Wd0)**	(Dastmalchi, et al., 2014)
21	217.0465 $[M+Na]^+$ ($C_{10}H_{10}O_4Na$) −5.5 ppm)	170,146, 121	**Ferulic acid** $C_{10}H_{10}O_4$ 194.0579	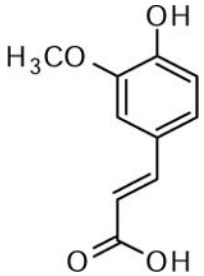	**Atlantic (Wd0), Norkotah Russet (Wd0) and Yukon Gold (Wd0)**	(Dastmalchi, et al., 2014)
22	$C_{16}H_{19}O_8$ $[M+H]^+$ 339.1070 (−1.18 ppm)	333, 239, 133	**Coumaroyl quinic acid** $C_{16}H_{18}O_8$ 338.0996	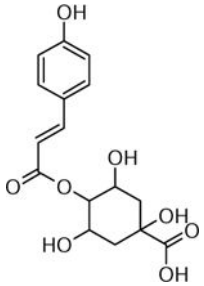	**Atlantic (Wd0, Wd1A)**	(Dastmalchi, et al., 2014)

Compou nd No.[a]	[M+H]+/[M-H]-or [M+Na] +	MS/MS Fragment ions (Positive)	Biomarker Formula and Molecular Weight	Structural Formula	Wound Time Point Specific Marker	References
23	335.1017 [M+H]+ $C_{16}H_{19}O_9$ (−1.97 ppm)	201, 163	**Caffeoylquinic acid** $C_{16}H_{18}O_9$ 354.0951	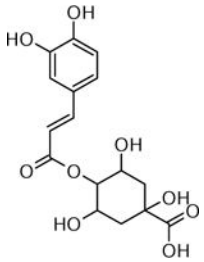	**Atlantic (Wd0), Norkotah Russet (Wd1) and Yukon Gold (Wd1)**	(Dastmalchi, et al., 2014)
24	$C_{17}H_{20}O_9Na$ [M+Na]+ 391.1026 (7.62 ppm)	325, 377, 177, 155, 133, 121	**Feruloyl quinic acid** $C_{17}H_{20}O_9$ 368.1107	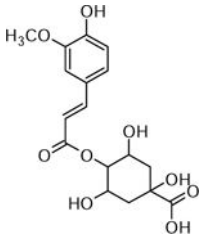	**Atlantic (Wd0)**	(Dastmalchi, et al., 2014)
25	$C_{14}H_{15}O_4$ [M+H]+ 245.0792 (7.62 ppm)	189, 149,121	**Piceatannol** $C_{14}H_{12}O_4$ 244.073	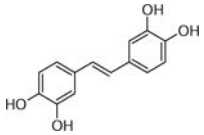	**Yukon (Wd0)**	(Cruz, et al., 2014)
Fatty acids and Fatty alcohol conjugates						
26	699.4351 [M+Na]+ $C_{37}H_{62}O_8Na$ (6.39 ppm)	369, 353, 295, 277	**Dicaffeoyl ester of trihydroxy-6,8,10,12-Eicosatetraenoic acid,**[b] $C_{37}H_{62}O_8$ 676.3301	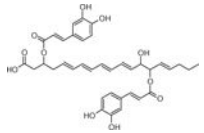	**Yukon Gold (Wd3)**	(Ricker & Bostock, 1994)
27	695.4358 [M+Na]+ $C_{37}H_{60}O_8Na$ (7.71 ppm)	351, 293, 275	**Dicaffeoyl ester of trihydroxy-Eicosapentaenoic acid**[b] $C_{37}H_{60}O_8$ 632.4283	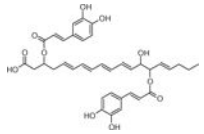	**Chipeta (Wd0)**	(Ricker & Bostock, 1994)

Compou nd No.[a]	$[M+H]^+/[M-H]^-$ or $[M+Na]^+$	MS/MS Fragment ions (Positive)	Biomarker Formula and Molecular Weight	Structural Formula	Wound Time Point Specific Marker	References
28	699.4351 $[M+Na]^+$ $C_{37}H_{62}O_8Na$ (6.39 ppm)	369, 353, 295, 277	**Dicaffeoyl ester of -trihydroxy-Eicosatetraenoic acid,** [b] $C_{37}H_{62}O_8$ 676.3301	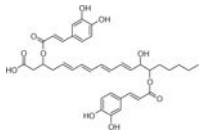	**Norkotah Russet (Wd7) Chipeta (Wd0)**	(Ricker & Bostock, 1994)
29	316.2844 $[M+H]^+$ $C_{18}H_{38}N_2O_3$ (0.63 ppm)	241, 194	**2-amino-8–1,3,4-triol, Octadecene** $C_{18}H_{37}N_2O_3$ 315.2768	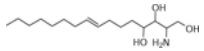	**Chipeta (Wd3)**	(Bartke, et al., 2006)

Compou nd No.[a]	$[M+H]^+/[M-H]^-$ or $[M+Na]^+$	MS/MS Fragment ions (Positive)	Biomarker Formula and Molecular Weight	Structural Formula	Wound Time Point Specific Marker	References
30	511.3384 $[M+Na]^+$ $C_{31}H_{52}O_4Na$ (7.3 ppm)	445, 361, 195	**Alkyl ferulate (C22:0)** $C_{31}H_{52}O_4$ 488.386	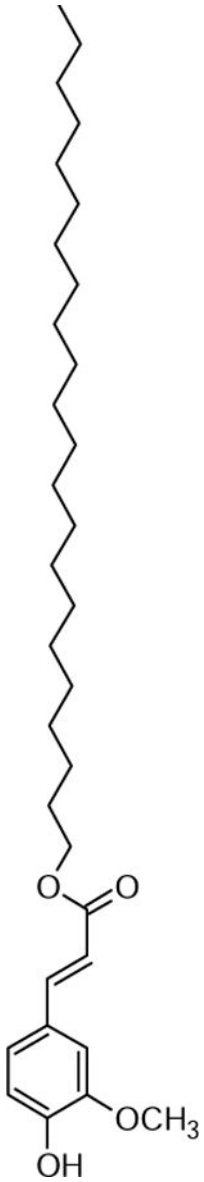	**Atlantic (Wd0)**	(Landgraf, et al., 2014)

Compou nd No.[a]	[M+H]+/[M-H]-or [M+Na] +	MS/MS Fragment ions (Positive)	Biomarker Formula and Molecular Weight	Structural Formula	Wound Time Point Specific Marker	References
31	527.3920 [M+Na]+ $C_{31}H_{52}O_5Na$ (4.03 ppm)	439,413 , 311, 195	**Hydroxy alkyl ferulate (C21:0)** $C_{31}H_{52}O_5$ 504.3854	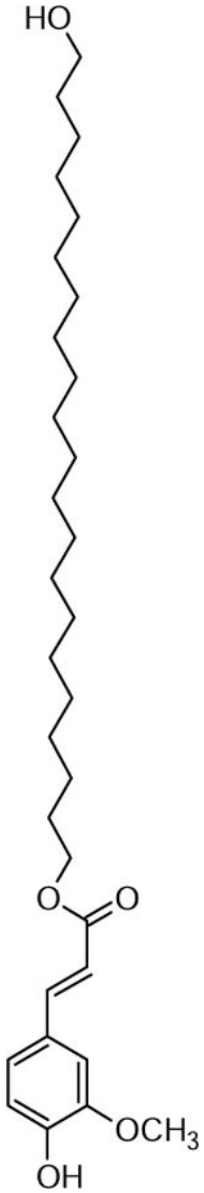	**Atlantic (Wd0)**	(Landgraf, et al., 2014)

Compou nd No.[a]	$[M+H]^+/[M-H]^-$ or $[M+Na]^+$	MS/MS Fragment ions (Positive)	Biomarker Formula and Molecular Weight	Structural Formula	Wound Time Point Specific Marker	References
Sterols						
32	1087.5285 $[M+K]^+C_{51}H_{84}O_{22}K$ (−18.11 ppm)	903, 753, 706, 560, 519	**Protodioscine** $C_{51}H_{84}O_{22}$ 1048.5644	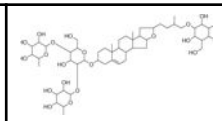	**Atlantic (Wd1)**	(Huang, et al., 2017)
33	1073.5470 $[M+Na]^+$ $C_{51}H_{86}O_{22}Na$ (−4.01 ppm)	727, 545, 471, 401, 383, 309, 255	**Dihydro-ASP-II** $C_{51}H_{86}O_{22}$ 1050.561	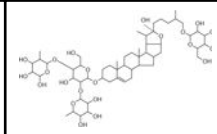	**Norkotah Russet (Wd3 and Wd7)**	(Huang, et al., 2017; Jin, et al., 2018)
34	963.5862 $C_{51}H_{89}O_{14}K$ (−6.65 ppm)	685,607, 430,311, 121	**22,25-dimethoxy-3-[[2,3,4-tri-O-methyl-6-O-(2,3, 4,6-tetra-O-methyl-β-D-glucopyranosyl)-β-D-glucopyranosyl] oxy]-, (3β)-lanost-9(11)-en-24-one** $C_{51}H_{89}O_{14}$ 924.6174	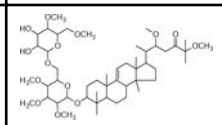	**Norkotah Russet (Wd0)**	(Dastmalchi, et al., 2016)
Glycoalkaloids						
35	852.5136 $[M+H]^+$ ($C_{45}H_{74}NO_{14}$ −3.7ppm)	722, 706, 560, 398	**α-Chaconine** $C_{45}H_{73}NO_{14}$ 851.5031	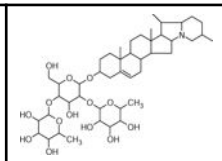	**Atlantic (Wd0)**	(Dastmalchi, et al., 2014)
36	884.4924 $[M+H]^+$ ($C_{45}H_{74}NO_{16}$ −9.2 ppm)	868, 722,704, 576, 414,396	**Leptinine II** $C_{45}H_{73}NO_{16}$ 883.4929	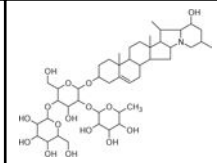	**Norkotah Russet (Wd2) and Atlantic (Wd2)**	(Dastmalchi, et al., 2014)
37	868.5044 $[M+H]^+$ ($C_{45}H_{74}NO_{15}$ −1.03 ppm)	850, 722, 704, 563, 414, 396	**Leptinine I** C45H73NO15 867.4980	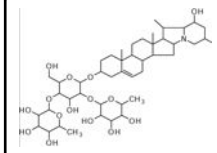	**Norkotah Russet (Wd7) Atlantic (Wd1)**	(Dastmalchi, et al., 2014)

Compou nd No.[a]	$[M+H]^+/[M-H]^-$ or $[M+Na]^+$	MS/MS Fragment ions (Positive)	Biomarker Formula and Molecular Weight	Structural Formula	Wound Time Point Specific Marker	References
38	868.5073 $[M+H]^+$ $C_{45}H_{74}NO_{15}$ (−2.03 ppm)	852, 722, 706, 560, 398	**α-Solanine** $C_{45}H_{73}NO_{15}$ 867.4980	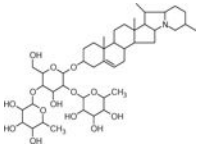	**Chipeta (Wd1) and Atlantic (Wd0)**	(Dastmalchi, et al., 2014; Huang, et al., 2017; Jin, et al., 2018)
39	884.4924 $[M+H]^+$ $C_{45}H_{74}NO_{16}$ (−9.2 ppm)	738, 722, 704,576, 414,396	**Solamarine** $C_{45}H_{73}NO_{16}$ 883.4929	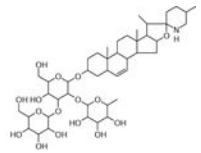	**Norkotah Russet (Wd7) and Atlantic (Wd7)**	(Shakya & Navaree, 2008)
40	1046.551 $[M+H]^+$ $C_{51}H_{84}NO_{21}$ (−2.03 ppm)	831, 698,610	**Dehydro commersonine** $C_{51}H_{83}NO_{21}$ 1045.5452	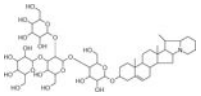	**Atlantic (Wd1)**	(Shakya & Navaree, 2008)

[a]Structures have been determined for 40 of the 42 identified marker compounds.

[b]Structures drawn are tentative as we could not ascertain the postion of hydroxy and double bonds based on the data available